Numerical calculation of the transfer of polarized radiation by a scattering and absorbing atmosphere

D. M. O'Brien

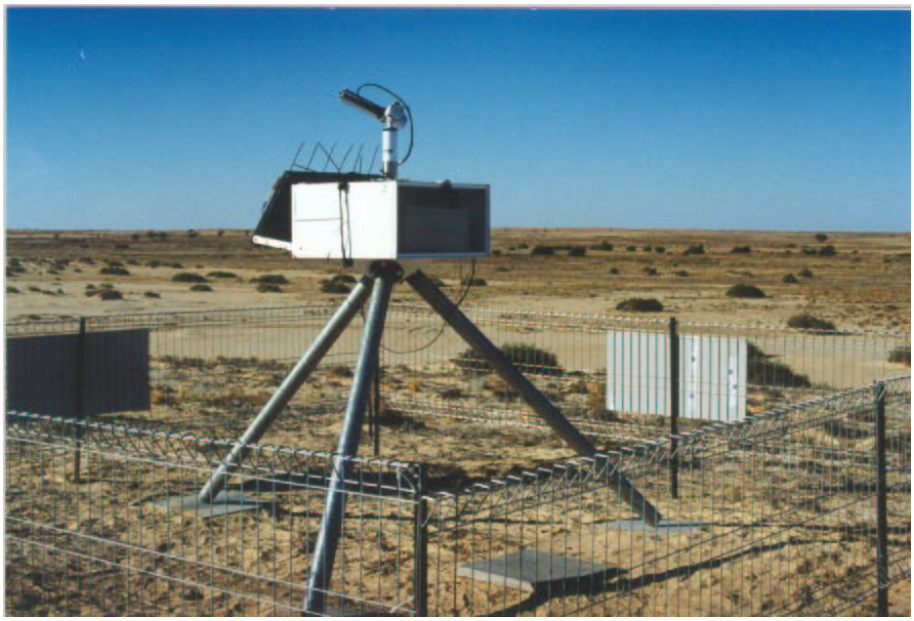

Atmospheric Research
CSIRO Atmospheric Research Technical Paper No. 49

National Library of Australia Cataloguing-in-Publication Entry

O'Brien, D.M. (Denis Michael), 1948-.

Numerical calculation of the transfer of polarized radiation by a scattering and absorbing atmosphere

ISBN 0 643 06640 3.

1. Radiative transfer. 2. Atmospheric radiation. I. CSIRO. Division of Atmospheric Research. II. Title. (Series: CSIRO Atmospheric Research technical paper; no. 49).

551.5271

This research was supported through the Australian Greenhouse Office.

CSIRO Atmospheric Research
PMB 1, Aspendale, Victoria 3195, Australia
Phone: (+61 3) 9239 4400; Fax: (+61 3) 9239 4444
E-mail: chief@dar.csiro.au

CSIRO Atmospheric Research Technical Papers may be issued out of sequence. From July 2000, all new Technical Papers will appear on the web site of CSIRO Atmospheric Research. Some Technical Papers will appear also in paper form. A complete list of CSIRO Atmospheric Research Technical Papers can be found at www.dar.csiro.au/info/TP.htm.

Contents

1 Introduction

Aerosols modify climate predominantly by scattering and absorption of the energy from the sun and by influencing the formation and lifetime of clouds. In both roles, the size, shape and chemical composition of the aerosol particles are important factors, so it may seem at first sight that an assessment of the risks associated with climate change should include the apparently impossible task of tracking the release and evolution in the atmosphere of particles with sub-micron sizes. Fortunately, research shows that the optical properties of aerosol may be characterized by relatively few parameters; the total number of particles, their refractive indices, an estimate of shape, and the area weighted mean and variance of the distribution of particle sizes. While considerable progress has been made in measuring these properties from space over the oceans, the same is not the case for observations over land. Progress is more difficult for land because the radiance scattered to space by aerosol is generally much smaller than the radiance reflected from the bright surface. Radiometers in space cannot distinguish reliably between these components, so estimates of aerosol properties based upon measurements of the scattered radiance are necessarily uncertain. Various strategies have been proposed to overcome these problems, usually with the common theme of reducing or eliminating the component of the radiance reflected from the surface. For example, multi-spectral observations that include a frequency where there is strong absorption by a well-mixed gas (such as oxygen) will reduce the surface component, leaving a clearer aerosol signature. Alternatively, with two views of the target taken a few minutes apart at different zenith angles (as with the Along Track Scanning Radiometer), the common component of the radiance reflected from the surface may be cancelled partially. Perhaps the most promising option is to measure not only the intensity of the radiation reflected to space but also its polarization, because polarization signatures of reflected and scattered light are markedly different. Such a strategy has been employed, for example, by POLDER on ADEOS (Deschamps et al., 1994).

Whatever the instrument in space, it is clear that a comprehensive validation program is required. This will involve sun-photometers to measure average aerosol properties over the entire atmospheric column, nephelometers to measure the scattering properties of near-surface air, and filter samplers to determine the chemical composition of aerosol particles, again in near surface air. Polarization also is important for surface measurements, because polarization is sensitive to particle shape. Furthermore, the horizontally polarized component of the radiance is symmetric about the zenith in the principal plane for a Rayleigh atmosphere, thereby allowing the radiance scattered by aerosol to be differentiated from that scattered by molecules.

In order to pursue the connection between radiance measured by satellites and sun-photometers on one hand and the optical properties of aerosol on the other, it is clear that a numerical model of the transfer of polarized radiation in the atmosphere is an essential tool, because the causal links between aerosol properties and radiance characteristics can be explored through numerical simulations. This report describes such a numerical model, documenting the structure of the model, its accuracy and test data. Application of the model will be the subject of later reports in this series.

The principal components of a typical radiation code are shown in figure 1, in which three stages are apparent:

1. the top three rows represent the synthesis of the optical properties of the atmosphere from its microphysical composition;

2. the loop denoted 'Spectral integration' involves repeated solution of the monochromatic radiative transfer equation (RTE) at frequencies within the band-pass of the

observing system;

3. within the spectral integration loop, the monochromatic radiance must be convolved with the response function of the observing system to simulate the measured quantities.

The general tasks of synthesis, solution and simulation are carried out by code developed by the author for separate projects at CSIRO Atmospheric Research (CAR), so this report focuses on the monochromatic RTE solver for polarized radiation. The design of the solver allows the new polarization features to be integrated seamlessly into the more general radiation package. Thus, the details of the synthesis and spectral integration, the latter carried out by correlated k-distributions, and the infrastructure to develop those distributions, will be reported separately.

Section 2 outlines the theory underlying the transfer of polarized radiation in the atmosphere. Although this material is not new scientifically, the formulation has some novel features, and the formulae are presented in a way that is compact, clear and well suited to computer code, thereby enhancing reliability. Section 3 describes the algorithm, which solves the RTE iteratively via the multiple scattering series. The algorithm is similar in form to that used by Mitchell et al. (1996), for unpolarized radiance. For thin atmospheres containing only molecules and aerosols, the rate of convergence is acceptable. Section 4 is concerned with the philosophy underlying the radiation code in general, and with the polarized RTE solver module in particular. The storage strategy and the data structures used in the code are defined. This section is not intended to be an exhaustive documentation of the code, but rather to provide sufficient insight to enable a user to follow the (well commented) code. Section 5 outlines comprehensive tests of the correctness of the code and its rate of convergence. Three cases are used for the tests, the first two involving thin ($\tau = 0.1$) and moderately thick ($\tau = 1$) Rayleigh atmospheres over non-reflecting and reflecting surfaces, while the third case involves both molecular and aerosol scattering, again over a reflecting surface. The final brief section 6 describes the transformations required to simulate the polarized radiances measured by Cimel sunphotometers, as deployed at Tinga Tingana, Alice Springs, Lake Argyle and Jabiru as part of this project.

2 Theoretical formulation

2.1 Polarization and scattering geometry

2.1.1 Stokes' vectors

The state of polarization is specified via the components of Stokes' vector (Stokes, 1852),

$$\mathcal{I} = \begin{pmatrix} I \\ Q \\ U \\ V \end{pmatrix}.$$

Components I, $(Q^2+U^2)^{1/2}$ and V are invariant under rotations of the coordinate system about the direction $\mathbf{r}$ of propagation of the photons, but Q and U depend upon the orientation with respect to a reference plane that includes $\mathbf{r}$. For photons propagating freely in direction $\mathbf{r}$, it is customary to define the plane of reference by $\mathbf{r}$ and $\mathbf{n}$, where $\mathbf{n}$ is a unit vector pointing vertically upwards. However, when photons scatter from

incident direction $\mathbf{r}$ to exit direction $\mathbf{r}'$, the plane of reference is taken to be the plane containing both $\mathbf{r}$ and $\mathbf{r}'$. Thus, when considering scattering, it is necessary to examine the transformation of Stokes' vectors under rotations of the coordinate axes. This section develops practical formulae for this purpose.

Because a radiation stream with an arbitrary state of polarization may be written as the sum of two independent streams of elliptically polarized radiation with opposite polarization (Chandrasekhar, 1950), it suffices to focus on elliptically polarized radiation. In this case, the radiance is expressed in the form

$$\begin{pmatrix} I \\ Q \\ U \\ V \end{pmatrix} = A^2 \begin{pmatrix} 1 \\ \cos 2\beta \, \cos 2\chi \\ \cos 2\beta \, \sin 2\chi \\ \sin 2\beta \end{pmatrix},$$

where A is the mean amplitude of the electric field vector, the semi-major and semi-minor axes of the polarization ellipse are $A\cos\beta$ and $A\sin\beta$, and χ is the inclination of the polarization ellipse relative to the reference plane (see figure 2).

2.1.2 Transformation of Stokes' vectors under coordinate rotations

The geometry is indicated in figures 2 and 3, where all direction vectors are assumed to be unit vectors. Vector $\mathbf{r}$ denotes the direction of propagation of the photons, vectors $\mathbf{q}$ and $\mathbf{r}$ define the reference plane for polarization, while vector $\mathbf{p}$ completes the right-handed orthonormal system. Consider a rotation of the reference plane about the direction of propagation through angle ζ, as shown in figure 3. The new reference plane is defined by vectors $\mathbf{q}'$ and $\mathbf{r}$. In the rotated (primed) coordinate frame the inclination of the polarization ellipse is $\chi - \zeta$, rather than χ as in the unprimed coordinates, so

$$\begin{aligned} Q' &= A^2 \cos 2\beta \, \cos 2(\chi - \zeta) \\ U' &= A^2 \cos 2\beta \, \sin 2(\chi - \zeta), \end{aligned}$$

which may be written after a little rearrangement as

$$\begin{pmatrix} Q' \\ U' \end{pmatrix} = \begin{pmatrix} \cos 2\zeta & \sin 2\zeta \\ -\sin 2\zeta & \cos 2\zeta \end{pmatrix} \begin{pmatrix} Q \\ U \end{pmatrix}.$$

Because

$$\begin{pmatrix} \cos 2\zeta & \sin 2\zeta \\ -\sin 2\zeta & \cos 2\zeta \end{pmatrix} = \begin{pmatrix} \cos\zeta & \sin\zeta \\ -\sin\zeta & \cos\zeta \end{pmatrix}^2,$$

Stokes' vectors in the original and rotated coordinate systems are related by

$$\mathcal{I}' = \begin{pmatrix} 1 & 0 & 0 \\ 0 & M & 0 \\ 0 & 0 & 1 \end{pmatrix}^2 \mathcal{I},$$

where

$$M = \begin{pmatrix} \cos\zeta & \sin\zeta \\ -\sin\zeta & \cos\zeta \end{pmatrix}.$$

In order to avoid the ambiguities of quadrant and sign that often accompany trigonometric calculations, we express all quantities in vector notation and perform only the invariant

operations of dot and cross products. To achieve this goal, note that

$$\begin{aligned}
\mathbf{p}\cdot\mathbf{p}' &= \cos\zeta,\\
\mathbf{p}\cdot\mathbf{q}' &= \cos(\pi/2-\zeta) = \sin\zeta,\\
\mathbf{q}\cdot\mathbf{p}' &= \cos(\pi/2+\zeta) = -\sin\zeta,\\
\mathbf{q}\cdot\mathbf{q}' &= \cos\zeta,
\end{aligned}$$

so the matrix M may be written

$$M = \begin{pmatrix} \mathbf{p}.\mathbf{p}' & \mathbf{p}.\mathbf{q}' \\ \mathbf{q}.\mathbf{p}' & \mathbf{q}.\mathbf{q}' \end{pmatrix} = \underbrace{\begin{pmatrix} \mathbf{p} \\ \mathbf{q} \end{pmatrix}}_{\text{old}} \cdot \underbrace{\begin{pmatrix} \mathbf{p}' & \mathbf{q}' \end{pmatrix}}_{\text{new}},$$

where 'old' and 'new' refer to the coordinate frames defining the reference planes. In this form, M depends on the scalar invariants formed from the vectors $\mathbf{p}$, $\mathbf{q}$, $\mathbf{p}'$ and $\mathbf{q}'$, and therefore is not tied to any particular coordinate representation.

2.1.3 Müller matrices

Consider a scattering process where photons enter on ray $\mathbf{r}_0$ and exit on ray $\mathbf{r}_1$. Let $\mathcal{I}'_0$ and $\mathcal{I}'_1$ denote Stokes' vectors for the incident and scattered photons, for both of which the reference plane of polarization is chosen to be the scattering plane, defined by the propagation vectors $\mathbf{r}_0$ and $\mathbf{r}_1$. The scattering event is described by a Müller matrix F,

$$\mathcal{I}'_1 = F\mathcal{I}'_0,$$

where F depends on the scattering angle ψ, defined by

$$\cos\psi = \mathbf{r}_0\cdot\mathbf{r}_1. \tag{1}$$

For example, for Rayleigh scattering the Müller matrix has the form

$$F = \tfrac{3}{4}\begin{pmatrix} 1+\cos^2\psi & 1-\cos^2\psi & 0 & 0 \\ 1-\cos^2\psi & 1+\cos^2\psi & 0 & 0 \\ 0 & 0 & 2\cos\psi & 0 \\ 0 & 0 & 0 & 2\cos\psi \end{pmatrix} \qquad \text{(Rayleigh)},$$

whereas for scattering by spherical particles it has the form

$$F = \begin{pmatrix} (M_2+M_1)/2 & (M_2-M_1)/2 & 0 & 0 \\ (M_2-M_1)/2 & (M_2+M_1)/2 & 0 & 0 \\ 0 & 0 & S_{21} & -D_{21} \\ 0 & 0 & D_{21} & S_{21} \end{pmatrix} \qquad \text{(Mie)}.$$

In the last expression, M_k, S_{jk} and D_{jk} are related to the complex scattering amplitude A_k via

$$\begin{aligned}
M_k &= |A_k|^2,\\
S_{jk} &= (A_jA_k^\star + A_kA_j^\star)/2,\\
D_{jk} &= -i(A_jA_k^\star - A_kA_j^\star)/2
\end{aligned}$$

(van de Hulst, 1981).

2.1.4 Transformation of the incident Stokes' vector

Let Q_0 and U_0 denote the coordinates of Stokes' vector for the incoming ray, for which the reference plane is defined by $\mathbf{r}_0$ and $\mathbf{n}$, the latter being a unit vector pointing vertically upwards. We introduce an orthonormal system of vectors, $\mathbf{p}_0$, $\mathbf{q}_0$ and $\mathbf{r}_0$, as follows:

$$\mathbf{p}_0 = \frac{\mathbf{n} \times \mathbf{r_0}}{|\mathbf{n} \times \mathbf{r_0}|} \qquad \text{and} \qquad \mathbf{q}_0 = \mathbf{r_0} \times \mathbf{p_0}. \tag{2}$$

Clearly, $\mathbf{p}_0$ is perpendicular to both $\mathbf{n}$ and $\mathbf{r}_0$, and therefore lies in the horizontal plane. Because the vector $\mathbf{q}_0$ lies in the reference plane determined by $\mathbf{n}$ and $\mathbf{r}_0$, vectors $\mathbf{q}_0$ and $\mathbf{r}_0$ provide an alternative definition of this plane.

However, in order to apply the Müller matrix to the incident Stokes' vector, the reference plane must be rotated about the propagation vector $\mathbf{r}_0$ so that the reference plane coincides with the scattering plane. In order to do so, define

$$\mathbf{p}_0' = \frac{\mathbf{r_1} \times \mathbf{r_0}}{|\mathbf{r_1} \times \mathbf{r_0}|} \qquad \text{and} \qquad \mathbf{q}_0' = \mathbf{r_0} \times \mathbf{p_0'},$$

as indicated in figure 4. In the coordinate frame with $\mathbf{q}_0'$ and $\mathbf{r}_0$ defining the reference plane (identical with the plane defined by $\mathbf{r}_0$ and $\mathbf{r}_1$), the coordinates of the incident Stokes' vector are

$$\begin{pmatrix} Q_0' \\ U_0' \end{pmatrix} = \left(\underbrace{\begin{pmatrix} \mathbf{p}_0 \\ \mathbf{q}_0 \end{pmatrix}}_{\text{old}} \cdot \underbrace{\begin{pmatrix} \mathbf{p}_0' & \mathbf{q}_0' \end{pmatrix}}_{\text{new}} \right)^2 \begin{pmatrix} Q_0 \\ U_0 \end{pmatrix} = \begin{pmatrix} \mathbf{p}_0 \cdot \mathbf{p}_0' & \mathbf{p}_0 \cdot \mathbf{q}_0' \\ \mathbf{q}_0 \cdot \mathbf{p}_0' & \mathbf{q}_0 \cdot \mathbf{q}_0' \end{pmatrix}^2 \begin{pmatrix} Q_0 \\ U_0 \end{pmatrix}.$$

Therefore, Stokes' vector for the incident beam, with the reference plane as the scattering plane, is given by

$$\mathcal{I}_0' = \begin{pmatrix} I_0' \\ Q_0' \\ U_0' \\ V_0' \end{pmatrix} = \begin{pmatrix} 1 & 0 & 0 & 0 \\ 0 & \mathbf{p}_0 \cdot \mathbf{p}_0' & \mathbf{p}_0 \cdot \mathbf{q}_0' & 0 \\ 0 & \mathbf{q}_0 \cdot \mathbf{p}_0' & \mathbf{q}_0 \cdot \mathbf{q}_0' & 0 \\ 0 & 0 & 0 & 1 \end{pmatrix}^2 \begin{pmatrix} I_0 \\ Q_0 \\ U_0 \\ V_0 \end{pmatrix}.$$

2.1.5 Stokes' vector after scattering

Stokes' vector $\mathcal{I}_1'$ for the scattered radiation, with the reference plane for polarization as the scattering plane, is obtained from $\mathcal{I}_0'$ by multiplication by the Müller matrix F:

$$\mathcal{I}_1' = F\mathcal{I}_0'.$$

2.1.6 Transformation of the scattered Stokes' vector

The final coordinate system has the reference plane for polarization defined by $\mathbf{n}$ and $\mathbf{r}_1$. In a manner analogous to that used for the incident beam, we define

$$\mathbf{p}_1 = \frac{\mathbf{n} \times \mathbf{r_1}}{|\mathbf{n} \times \mathbf{r_1}|} \qquad \text{and} \qquad \mathbf{q}_1 = \mathbf{r_1} \times \mathbf{p_1}, \tag{3}$$

so that $\mathbf{p}_1$, $\mathbf{q}_1$ and $\mathbf{r}_1$ are orthonormal, and $\mathbf{q}_1$ and $\mathbf{r}_1$ define the reference plane for polarization. We also define

$$\mathbf{p}_1' = \frac{\mathbf{r_0} \times \mathbf{r_1}}{|\mathbf{r_0} \times \mathbf{r_1}|} = -\mathbf{p}_0' \qquad \text{and} \qquad \mathbf{q}_1' = \mathbf{r_1} \times \mathbf{p_1'},$$

as indicated in figure 5. Stokes' vector for the scattered beam with reference plane defined by $\mathbf{n}$ and $\mathbf{r}_1$ is related to Stokes' vector with the plane of scattering as the reference plane by

$$\begin{pmatrix} Q_1 \\ U_1 \end{pmatrix} = \left(\underbrace{\begin{pmatrix} \mathbf{p}_1' \\ \mathbf{q}_1' \end{pmatrix}}_{\text{old}} \cdot \underbrace{\begin{pmatrix} \mathbf{p}_1 & \mathbf{q}_1 \end{pmatrix}}_{\text{new}} \right)^2 \begin{pmatrix} Q_1' \\ U_1' \end{pmatrix} = \begin{pmatrix} \mathbf{p}_1' \cdot \mathbf{p}_1 & \mathbf{p}_1' \cdot \mathbf{q}_1 \\ \mathbf{q}_1' \cdot \mathbf{p}_1 & \mathbf{q}_1' \cdot \mathbf{q}_1 \end{pmatrix}^2 \begin{pmatrix} Q_1' \\ U_1' \end{pmatrix},$$

from which we obtain

$$\mathcal{I}_1 = \begin{pmatrix} 1 & 0 & 0 & 0 \\ 0 & \mathbf{p}_1' \cdot \mathbf{p}_1 & \mathbf{p}_1' \cdot \mathbf{q}_1 & 0 \\ 0 & \mathbf{q}_1' \cdot \mathbf{p}_1 & \mathbf{q}_1' \cdot \mathbf{q}_1 & 0 \\ 0 & 0 & 0 & 1 \end{pmatrix}^2 \mathcal{I}_1'.$$

2.1.7 Scattering matrix

The entire process by which $\mathcal{I}_0$ is transformed to $\mathcal{I}_1$ is represented by a scattering matrix P,

$$\mathcal{I}_1 = P\mathcal{I}_0. \tag{4}$$

Combining the preceding steps, we see that P is the product of the rotation matrix for the incident Stokes' vector, the Müller matrix defined in the scattering plane, and the final rotation matrix for the scattered Stokes' vector,

$$P = \begin{pmatrix} 1 & 0 & 0 & 0 \\ 0 & \mathbf{p}_1' \cdot \mathbf{p}_1 & \mathbf{p}_1' \cdot \mathbf{q}_1 & 0 \\ 0 & \mathbf{q}_1' \cdot \mathbf{p}_1 & \mathbf{q}_1' \cdot \mathbf{q}_1 & 0 \\ 0 & 0 & 0 & 1 \end{pmatrix}^2 F \begin{pmatrix} 1 & 0 & 0 & 0 \\ 0 & \mathbf{p}_0 \cdot \mathbf{p}_0' & \mathbf{p}_0 \cdot \mathbf{q}_0' & 0 \\ 0 & \mathbf{q}_0 \cdot \mathbf{p}_0' & \mathbf{q}_0 \cdot \mathbf{q}_0' & 0 \\ 0 & 0 & 0 & 1 \end{pmatrix}^2. \tag{5}$$

2.1.8 Summary

The equations developed here use only vector operations of dot and cross products. Not only is this conceptually cleaner, but also the equations in vector form are less prone to error when coded. In practice we define the vectors initially in Cartesian coordinates, but thereafter all operations are performed on three-dimensional vectors using only dot and cross products. The task of computing the scattered radiance breaks down into the following steps.

1. Given are the Stokes' vector $\mathcal{I}_0$, the incident direction $\mathbf{r}_0$ and the exit direction $\mathbf{r}_1$. The reference plane for the incident beam is defined by $\mathbf{n}$ and $\mathbf{r}_0$, while that for the scattered beam is defined by $\mathbf{n}$ and $\mathbf{r}_1$. Here $\mathbf{n}$ is any fixed direction in space, but in practice is chosen to be a unit vector pointing vertically upwards.

2. Compute $\mathbf{p}_0$ and $\mathbf{q}_0$ from equation (2).

3. Compute the Müller matrix for scattering angle ψ, defined in terms of $\mathbf{r}_0$ and $\mathbf{r}_1$ by equation (1).

4. Compute $\mathbf{p}_1$ and $\mathbf{q}_1$ from equation (3).

5. Compute the dot products as required by the scattering matrix in equation (5), thereby ensuring independence of coordinate frame, and then compute $\mathcal{I}_1$ from equation (4).

2.2 Optical properties of the atmosphere

The atmosphere is assumed to be a mixture of several constituents, indexed by r. The optical properties of the r^{th} constituent are characterized by the specific absorption, scattering and extinction coefficients, a_r, b_r and c_r, and the scattering matrix P_r. The specific absorptions refer to absorption per unit mass, which we take to be the mole in the case of gases. If ρ_r denotes the density of the r^{th} constituent, expressed in units of $\mathrm{mol\,m^{-3}}$, then the absorption, scattering and extinction coefficients corresponding to the specific quantities are

$$\alpha_r = \rho_r a_r, \qquad \beta_r = \rho_r b_r \qquad \text{and} \qquad \gamma_r = \rho_r c_r.$$

The absorption, scattering and extinction coefficients per unit volume of the atmosphere, regarded as an ensemble of its constituents, are

$$\alpha = \sum_r \alpha_r, \qquad \beta = \sum_r \beta_r \qquad \text{and} \qquad \gamma = \sum_r \gamma_r,$$

while the specific coefficients are

$$a = \alpha/\rho, \qquad b = \beta/\rho, \qquad \text{and} \qquad c = \gamma/\rho,$$

where

$$\rho = \sum_r \rho_r$$

is the total density. Finally, the single scattering albedo ϖ and the composite scattering matrix for the atmosphere are

$$\varpi = \beta/\gamma \qquad \text{and} \qquad P = \beta^{-1} \sum_r \beta_r P_r.$$

2.3 Radiative transfer equation (RTE)

2.3.1 RTE for a plane parallel medium

The polarized radiance $\mathcal{I}(\mathbf{x}, \mathbf{s})$ at a point specified by the three-dimensional vector $\mathbf{x}$ and direction by unit vector $\mathbf{s}$ satisfies the radiative transfer equation (RTE),

$$\mathbf{s} \cdot \nabla \mathcal{I}(\mathbf{x}, \mathbf{s}) = -\gamma(\mathbf{x}) \mathcal{I}(\mathbf{x}, \mathbf{s}) + \beta(\mathbf{x}) \int_\Omega d\omega(\mathbf{s}')\, P(\mathbf{x}, \mathbf{s}, \mathbf{s}') \mathcal{I}(\mathbf{x}, \mathbf{s}'),$$

where $d\omega(\mathbf{s}')$ is the solid angle measure on the unit sphere Ω, normalized so that

$$\int_\Omega d\omega(\mathbf{s}') = 1.$$

In a plane-parallel medium, where the radiance depends only on height z and the polar angles (θ, φ) of unit vector $\mathbf{s}$,

$$\mathcal{I}(\mathbf{x}, \mathbf{s}) \to \mathcal{I}(z, \theta, \varphi),$$

and the directional derivative reduces to

$$\mathbf{s} \cdot \nabla \mathcal{I} \to \mu \frac{\partial}{\partial z} \mathcal{I},$$

where

$$\mu = \cos\theta,$$

so the RTE adopts the simple form

$$\mu \frac{\partial}{\partial z} \mathcal{I} = -\gamma \mathcal{I} + \beta \int_{\Omega} d\omega \, P\mathcal{I}, \tag{6}$$

in which the dependence upon the independent variables has been suppressed for clarity. If $\tau(z)$ denotes the optical path length from height z to space along a vertical ray, as shown in figure 6,

$$\tau(z) = \int_{z}^{\infty} dz' \, \gamma(z'),$$

then division of equation (6) by $\gamma(z)$ allows the independent variable to be changed from z to τ, leading to

$$\mu \frac{\partial}{\partial \tau} \mathcal{I} = \mathcal{I} - \varpi \int_{\Omega} d\omega \, P\mathcal{I}, \tag{7}$$

since

$$\gamma(z)^{-1} \frac{\partial}{\partial z} f(z) = -\frac{\partial}{\partial \tau} f(\tau)$$

for any function f. Henceforth, optical thickness τ will be used as the vertical coordinate instead of height.

2.3.2 Solar radiance

The solar radiance is a near singular source, and therefore requires special attention if the numerical scheme is to be accurate. We follow the usual practice of separating the radiance into the solar radiance $\mathcal{I}_\star$ and the diffuse radiance $\mathcal{D}$,

$$\mathcal{I} = \mathcal{I}_\star + \mathcal{D},$$

where $\mathcal{I}_\star$ is required to satisfy

$$\mu \frac{\partial}{\partial \tau} \mathcal{I}_\star = \mathcal{I}_\star. \tag{8}$$

Subtraction of equation (8) from equation (7) leads to

$$\mu \frac{\partial}{\partial \tau} \underbrace{(\mathcal{I} - \mathcal{I}_\star)}_{\substack{\text{Diffuse} \\ \text{radiance}}} = (\mathcal{I} - \mathcal{I}_\star) - \varpi \int_{\Omega} d\omega \, P(\mathcal{I} - \mathcal{I}_\star) - \varpi \underbrace{\int_{\Omega} d\omega \, P\mathcal{I}_\star}_{\substack{\text{Solar} \\ \text{source}}},$$

and hence to the following equation for the diffuse radiance,

$$\mu \frac{\partial}{\partial \tau} \mathcal{D} = \mathcal{D} - \varpi \int_{\Omega} d\omega \, P\mathcal{D} - \varpi \mathcal{S}, \tag{9}$$

in which $\mathcal{S}$, defined by

$$\mathcal{S} = \int_{\Omega} d\omega \, P\mathcal{I}_\star,$$

denotes the solar source.

There is some flexibility in choosing a solution of equation (8) to represent the solar radiance. Here we assume that $\mathcal{I}_\star$ has two components, the first representing the downward solar beam and the second the radiance produced by reflection of the solar beam at the surface. Neither component involves scattered photons, so $\mathcal{I}_\star$ also may be called the 'direct radiance'. The form of $\mathcal{I}_\star$ and the corresponding solar source $\mathcal{S}$ will be specified later when the boundary conditions are discussed.

2.3.3 Separation into upward and downward components

Define for any function $f(\mu)$

$$f^+(\mu) = \begin{cases} f(\mu) & \text{if } \mu > 0, \\ 0 & \text{if } \mu \le 0, \end{cases} \qquad \text{and} \qquad f^-(\mu) = \begin{cases} 0 & \text{if } \mu > 0, \\ f(\mu) & \text{if } \mu \le 0, \end{cases}$$

and specifically

$$\mathcal{D}^+(\tau,\mu,\varphi) = \begin{cases} \mathcal{D}(\tau,\mu,\varphi) & \text{if } \mu > 0, \\ 0 & \text{if } \mu \le 0, \end{cases} \qquad \text{and} \qquad \mathcal{D}^-(\tau,\mu,\varphi) = \begin{cases} 0 & \text{if } \mu > 0, \\ \mathcal{D}(\tau,\mu,\varphi) & \text{if } \mu \le 0. \end{cases}$$

Then

$$\begin{aligned} \mu\frac{\partial \mathcal{D}^+}{\partial \tau} &= \mathcal{D}^+ - \varpi\mathcal{S}^+ \qquad - \frac{\varpi}{4\pi}\int_{-1}^{1} d\mu' \int_0^{2\pi} d\varphi'\, P(\tau,\mu,\varphi,\mu',\varphi')\mathcal{D}(\tau,\mu',\varphi') \\ &= \mathcal{D}^+ - \varpi\mathcal{S}^+ \qquad - \frac{\varpi}{4\pi}\int_{-1}^{0} d\mu' \int_0^{2\pi} d\varphi'\, P^{+-}(\tau,\mu,\varphi,\mu',\varphi')\mathcal{D}^-(\tau,\mu',\varphi') \\ &\qquad\qquad\qquad - \frac{\varpi}{4\pi}\int_{0}^{1} d\mu' \int_0^{2\pi} d\varphi'\, P^{++}(\tau,\mu,\varphi,\mu',\varphi')\mathcal{D}^+(\tau,\mu',\varphi'), \end{aligned} \tag{10}$$

where

$$P^{\varepsilon\varepsilon'}(\tau,\mu,\varphi,\mu',\varphi') = \begin{cases} P(\tau,\mu,\varphi,\mu',\varphi') & \text{if } \varepsilon\mu > 0 \text{ and } \varepsilon'\mu' > 0, \\ 0 & \text{otherwise,} \end{cases}$$

with $\varepsilon = \pm$ and $\varepsilon' = \pm$. Similarly,

$$\begin{aligned} \mu\frac{\partial \mathcal{D}^-}{\partial \tau} &= \mathcal{D}^- - \varpi\mathcal{S}^- \qquad - \frac{\varpi}{4\pi}\int_{-1}^{0} d\mu' \int_0^{2\pi} d\varphi'\, P^{--}(\tau,\mu,\varphi,\mu',\varphi')\mathcal{D}^-(\tau,\mu',\varphi') \\ &\qquad\qquad\qquad - \frac{\varpi}{4\pi}\int_{0}^{1} d\mu' \int_0^{2\pi} d\varphi'\, P^{-+}(\tau,\mu,\varphi,\mu',\varphi')\mathcal{D}^+(\tau,\mu',\varphi'). \end{aligned} \tag{11}$$

Equations (10) and (11) may be written in the form

$$\mu\frac{\partial \mathcal{D}^+}{\partial \tau} = \mathcal{D}^+ - \varpi\mathcal{S}^+ - \varpi\mathcal{P}^{++}\mathcal{D}^+ - \varpi\mathcal{P}^{+-}\mathcal{D}^- \tag{12a}$$

$$\mu\frac{\partial \mathcal{D}^-}{\partial \tau} = \mathcal{D}^- - \varpi\mathcal{S}^- - \varpi\mathcal{P}^{-+}\mathcal{D}^+ - \varpi\mathcal{P}^{--}\mathcal{D}^-, \tag{12b}$$

where $\mathcal{P}^{\varepsilon\varepsilon'}$ is the integral operator with kernel $P^{\varepsilon\varepsilon'}(\tau,\mu,\varphi,\mu',\varphi')$, and even more compactly as

$$\begin{pmatrix} 1-\mu\dfrac{\partial}{\partial\tau} & 0 \\ 0 & 1-\mu\dfrac{\partial}{\partial\tau} \end{pmatrix} \begin{pmatrix} \mathcal{D}^+ \\ \mathcal{D}^- \end{pmatrix} = \varpi \begin{pmatrix} \mathcal{S}^+ \\ \mathcal{S}^- \end{pmatrix} + \varpi \begin{pmatrix} \mathcal{P}^{++} & \mathcal{P}^{+-} \\ \mathcal{P}^{-+} & \mathcal{P}^{--} \end{pmatrix} \begin{pmatrix} \mathcal{D}^+ \\ \mathcal{D}^- \end{pmatrix} \tag{12c}$$

or

$$\boldsymbol{\mathcal{A}\mathcal{D}} = \varpi\boldsymbol{\mathcal{S}} + \varpi\boldsymbol{\mathcal{P}\mathcal{D}} \tag{12d}$$

with the obvious assignments.

2.3.4 Solar source and boundary conditions

Two boundary conditions are required to ensure that the solution of the integro-differential RTE is determinate.

At the surface, the upward and downward components of the radiance are related by

$$\mathcal{I}^+ = \mathcal{R}^{+-}\mathcal{I}^-, \tag{13}$$

where the integral operator $\mathcal{R}^{+-}$ denotes the polarized reflectance of the surface, which is assumed to be known. The kernel of $\mathcal{R}^{+-}$ is $R^{+-}(\mu, \varphi, \mu', \varphi')$ the polarized bidirectional reflectance distribution function, so the explicit form of equation (13) is

$$\mathcal{I}^+(\tau_L, \mu, \varphi) = \frac{1}{4\pi} \int_{-1}^{0} d\mu' \int_{0}^{2\pi} d\varphi' \, R^{+-}(\mu, \varphi, \mu', \varphi')\mathcal{I}^-(\tau_L, \mu', \varphi'), \tag{14}$$

where τ_L denotes the total optical thickness of the atmosphere. We require that the solar radiance $\mathcal{I}_\star$ and the diffuse radiance $\mathcal{D}$ satisfy equation (14) separately. The solar radiance, now determined uniquely from equation (8), has two components,

$$\mathcal{I}_\star = \mathcal{B}_\star + \mathcal{C}_\star,$$

where the first represents the downward solar beam, and the second, defined by

$$\mathcal{C}_\star^+ = \exp((\tau - \tau_L)/\mu)\mathcal{R}^{+-}\mathcal{B}_\star^-(\tau_L) \qquad \text{and} \qquad \mathcal{C}_\star^- = 0,$$

represents the radiance arising from reflection of the downward solar beam at the surface. The explicit form for the solar beam is

$$\mathcal{B}_\star(\tau, \mu, \phi) = \mathcal{F}_\star \exp(\tau/\mu_\star)\delta(\mathbf{s}, \mathbf{s}_\star), \tag{15}$$

where $\mathbf{s}_\star$ is the direction of the solar beam, specified by zenith angle $\theta_\star$ and azimuth $\varphi_\star$,

$$\mu_\star = \cos\theta_\star,$$

and $\mathcal{F}_\star$ is determined by the boundary condition at the top of the atmosphere. For unpolarized, natural light from the sun,

$$\mathcal{F}_\star = \frac{F_\star}{4\pi} \begin{pmatrix} 1 \\ 0 \\ 0 \\ 0 \end{pmatrix},$$

where $F_\star$ is the flux density at the top of the atmosphere incident upon a surface perpendicular to the solar beam, and where the second factor represents the unit Stokes' vector of unpolarized radiation. From equation (15) it follows easily that

$$\mathcal{C}_\star^+(\tau, \mu, \varphi) = \exp((\tau - \tau_L)/\mu)\exp(\tau_L/\mu_\star)R^{+-}(\mu, \varphi, \mu_\star, \varphi_\star)\mathcal{F}_\star. \tag{16}$$

As a result of this definition for $\mathcal{I}_\star$, the diffuse radiance satisfies

$$\mathcal{D}^+(\tau_L, \mu, \varphi) = \frac{1}{4\pi} \int_{-1}^{0} d\mu' \int_{0}^{2\pi} d\varphi' \, R^{+-}(\mu, \varphi, \mu', \varphi')\mathcal{D}^-(\tau_L, \mu', \varphi'), \tag{17}$$

and so provides one boundary condition for equation (12a).

The second boundary condition for the RTE assumes that the sole source of illumination of the atmosphere is the sun. Consequently, the downward diffuse radiance $\mathcal{D}^-$ must vanish at the top of the atmosphere, thereby providing a boundary condition for equation (12b).

The solar source source term takes the form

$$\mathcal{S} = \int_\Omega d\omega\, P(\mathcal{B}_\star + \mathcal{C}_\star) = \mathcal{S}_\mathcal{B} + \mathcal{S}_\mathcal{C},$$

where

$$\mathcal{S}_\mathcal{B}(\tau, \mu, \varphi) = \exp(\tau/\mu_\star) P(\tau, \mu, \varphi, \mu_\star, \varphi_\star) \mathcal{F}_\star$$

and

$$\mathcal{S}_\mathcal{C}(\tau, \mu, \varphi) = \frac{1}{4\pi} \int_0^1 d\mu' \int_0^{2\pi} d\varphi'\, P(\tau, \mu, \varphi, \mu', \varphi') \mathcal{C}_\star(\tau, \mu', \varphi'). \tag{18}$$

The integration in equation (18) is restricted to the upward hemisphere, because $\mathcal{C}_\star^-$ is zero. Explicitly, the upward and downward components of the solar source are

$$\begin{aligned} \mathcal{S}_\mathcal{B}^+(\tau, \mu, \varphi) &= \exp(\tau/\mu_\star) P^{+-}(\tau, \mu, \varphi, \mu_\star, \varphi_\star) \mathcal{F}_\star \\ \mathcal{S}_\mathcal{B}^-(\tau, \mu, \varphi) &= \exp(\tau/\mu_\star) P^{--}(\tau, \mu, \varphi, \mu_\star, \varphi_\star) \mathcal{F}_\star, \end{aligned} \tag{19}$$

and

$$\begin{aligned} \mathcal{S}_\mathcal{C}^+(\tau, \mu, \varphi) &= \frac{1}{4\pi} \int_0^1 d\mu' \int_0^{2\pi} d\varphi'\, P^{++}(\tau, \mu, \varphi, \mu', \varphi') \mathcal{C}_\star^+(\tau, \mu', \varphi'), \\ \mathcal{S}_\mathcal{C}^-(\tau, \mu, \varphi) &= \frac{1}{4\pi} \int_0^1 d\mu' \int_0^{2\pi} d\varphi'\, P^{-+}(\tau, \mu, \varphi, \mu', \varphi') \mathcal{C}_\star^+(\tau, \mu', \varphi'). \end{aligned} \tag{20}$$

Note that $\mu_\star$ is negative in the above equations, so exponentials such as $\exp(\tau/\mu_\star)$ decrease with increasing optical thickness.

Although the formulation of equation (14) and equation (17) specifically excludes specular reflection, it is straightforward to reformulate the equations to include this effect. Finally, the simpler term 'reflectance' will be used instead of 'bidirectional reflectance distribution function' or BRDF.

2.4 Iterative algorithm

The algorithm solves equation (12c) by iteration, ensuring at every step that the boundary conditions are satisfied. The algorithm begins with an intial guess $\boldsymbol{\mathcal{D}}_0 = 0$ for the scattered radiance, and subsequently updates the estimate $\boldsymbol{\mathcal{D}}_k$ at the k^{th} iteration to $\boldsymbol{\mathcal{D}}_{k+1}$ by the following steps.

1. The downward component of $\mathcal{D}_{k+1}^-$ is defined in terms of $\boldsymbol{\mathcal{D}}_k$ by

$$\mu \frac{\partial \mathcal{D}_{k+1}^-}{\partial \tau} = \mathcal{D}_k^- - \varpi \mathcal{S}^- - \varpi \mathcal{P}^{-+} \mathcal{D}_k^+ - \varpi \mathcal{P}^{--} \mathcal{D}_k^-. \tag{21}$$

   The boundary condition for equation (21) is that $\mathcal{D}_{k+1}^-$ must be zero at the top of the atmosphere. Using this condition and the known value of $\boldsymbol{\mathcal{D}}_k$, the differential equation may be integrated downwards to the surface.

2. At the surface $\mathcal{D}^+_{k+1}$ is related to the downward diffuse radiance $\mathcal{D}^-_{k+1}$ via

$$\mathcal{D}^+_{k+1}(\tau_L,\mu,\varphi) = \frac{1}{4\pi}\int_{-1}^{0} d\mu' \int_{0}^{2\pi} d\varphi'\, R^{+-}(\mu,\varphi,\mu',\varphi')\mathcal{D}^-_{k+1}(\tau_L,\mu',\varphi'), \qquad (22)$$

so the boundary condition at the surface is satisfied by $\boldsymbol{\mathcal{D}}_{k+1}$.

3. The upward component of $\boldsymbol{\mathcal{D}}_{k+1}$ is defined in terms of $\mathcal{D}^-_{k+1}$ and $\mathcal{D}^+_k$ by

$$\mu\frac{\partial\mathcal{D}^+_{k+1}}{\partial\tau} = \mathcal{D}^+_k - \varpi\mathcal{S}^+ - \varpi\mathcal{P}^{++}\mathcal{D}^+_k - \varpi\mathcal{P}^{+-}\mathcal{D}^-_{k+1}. \qquad (23)$$

Because $\mathcal{D}^+_{k+1}$ is known at the surface equation (23) may be integrated upwards to find $\mathcal{D}^+_{k+1}$ at all levels. Note that equation (23) uses $\mathcal{D}^-_{k+1}$ rather than $\mathcal{D}^-_k$ in the integration over the downward diffuse radiance.

This iterative procedure ensures that the boundary conditions at the top of the atmosphere and at the surface are satisfied at every iteration. Furthermore, the sequence of iterates is a Cauchy sequence in the space of square integrable functions, so the sequence converges. The crucial point in proving these results (not detailed here) is that the operator $\boldsymbol{\mathcal{A}}^{-1}\boldsymbol{\mathcal{P}}$ (or one of its powers) is bounded above by unity. This occurs if the medium has finite optical thickness or if the single scattering albedo is less than unity, as occurs in the presence of absorption.

3 Numerical implementation

This section decribes the implementation of the algorithm for a layered medium, as shown in figure 7. The levels are labelled from the top downwards, with level 0 at the top of the atmosphere. The levels separate the layers, which are indexed from 1 to L. Optical thickness τ is measured from the top of the atmosphere downwards. We let τ_l denote the optical thickness from the top of the atmosphere to level l. The subscript k formerly used to index the iterates will be omitted henceforth for clarity, but a new subscript l will be added to all fields to indicate the level at which they are evaluated. Single-scattering albedo and the scattering matrix are assumed to be evaluated at the mid-points of the layers, which points will be denoted by index $(l-1/2)$.

3.1 Downward recursion

Let $\mathcal{D}^-_l$ denote the value of $\mathcal{D}^-(\tau,\mu,\varphi)$ at level l where $\tau=\tau_l$. In equation (12b) replace the derivative

$$\frac{\partial\mathcal{D}^-}{\partial\tau} \qquad \text{by the finite difference} \qquad \frac{\mathcal{D}^-_{l+1}-\mathcal{D}^-_l}{\delta\tau_l},$$

where $\delta\tau_l = \tau_{l+1}-\tau_l$ is the optical thickness of layer $(l+1)$, and on the right-hand side replace

$$\mathcal{D}^- \qquad \text{by the mean value} \qquad \frac{\mathcal{D}^-_{l+1}+\mathcal{D}^-_l}{2}.$$

Hence,

$$\mu\Big(\frac{\mathcal{D}^-_{l+1}-\mathcal{D}^-_l}{\delta\tau_l}\Big) = \Big(\frac{\mathcal{D}^-_{l+1}+\mathcal{D}^-_l}{2}\Big) - \mathcal{Q}^-_{l+1/2},$$

where

$$\mathcal{Q}^-_{l+1/2} \qquad \text{is the approximation to} \qquad \varpi(\mathcal{S}^- + \mathcal{P}^{-+}\mathcal{D}^+ + \mathcal{P}^{--}\mathcal{D}^-) \tag{24}$$

at the mid-point of layer $(l+1)$. Equation (24) can be rearranged to give

$$\mathcal{D}^-_{l+1} = \mathcal{D}^-_l + K^-_l(\mathcal{D}^-_l - \mathcal{Q}^-_{l+1/2}) \qquad \text{where} \qquad K^-_l = \frac{\delta\tau_l}{\mu - \delta\tau_l/2}. \tag{25}$$

At the top of the atmosphere, the downward diffuse radiance $\mathcal{D}^-_0$ is zero, which allows $\mathcal{D}^-_1$ to be computed from the source function $\mathcal{Q}^-_{1/2}$. From $\mathcal{D}^-_1$ may be computed $\mathcal{D}^-_2$, and so on down to the surface.

3.2 Surface reflection

The upward diffuse radiance at the surface is obtained from the downward diffuse radiance $\mathcal{D}^-$ and the (polarized) reflectance matrix for the surface. If the surface does not have a specularly reflecting component, then

$$\mathcal{D}^+_L(\mu,\varphi) = \frac{1}{4\pi}\int_{-1}^{0} d\mu' \int_{0}^{2\pi} d\varphi'\, R^{+-}(\mu,\varphi,\mu',\varphi')\mathcal{D}^-_L(\mu',\varphi').$$

The reflection operator $\mathcal{R}^{+-}$ with kernel $R^{+-}(\mu,\varphi,\mu',\varphi')$ must be specified *a priori*.

The particular case of Lambertian reflection should be mentioned here, as this is the case used in the tests. The criteria for Lambertian reflection are that:

1. the reflected radiance should be isotropic;
2. the reflected radiance should be unpolarized, no matter what the polarization of the incident radiance;
3. the ratio of the reflected flux density to the incident flux density at the surface should equal the albedo A specified for the surface.

It is easy to see that these criteria are met if

$$R^{+-}(\mu,\phi,\mu',\phi') = 4A\mu' \begin{pmatrix} 1 & 0 & 0 & 0 \\ 0 & 0 & 0 & 0 \\ 0 & 0 & 0 & 0 \\ 0 & 0 & 0 & 0 \end{pmatrix}.$$

3.3 Upward recursion

The equation

$$\mu\frac{\partial\mathcal{D}^+}{\partial\tau} = \mathcal{D}^+ - \mathcal{Q}^+$$

for the upward radiance is processed similarly. In this case, the upward radiance is known at the surface, so the recurrence relation may be used to calculate the upward radiance at all levels up to the top of the atmosphere.

Let $\mathcal{D}^+_l$ denote the value of $\mathcal{D}^+(\tau,\mu,\varphi)$ at the level l where $\tau = \tau_l$. In equation (12a) replace the derivative

$$\frac{\partial\mathcal{D}^+}{\partial\tau} \qquad \text{by the finite difference} \qquad \frac{\mathcal{D}^+_{l+1} - \mathcal{D}^+_l}{\delta\tau_l},$$

and on the right-hand side replace

$$\mathcal{D}^+ \qquad \text{by the mean value} \qquad \frac{\mathcal{D}^+_{l+1} + \mathcal{D}^+_l}{2}.$$

Hence,

$$\mu\Big(\frac{\mathcal{D}^+_{l+1} - \mathcal{D}^+_l}{\delta\tau_l}\Big) = \Big(\frac{\mathcal{D}^+_{l+1} + \mathcal{D}^+_l}{2}\Big) - \mathcal{Q}^+_{l+1/2},$$

where

$$\mathcal{Q}^+_{l+1/2} \qquad \text{is the approximation to} \qquad \varpi(\mathcal{S}^+ + \mathcal{P}^{++}\mathcal{D}^+ + \mathcal{P}^{+-}\mathcal{D}^-) \tag{26}$$

at the mid-point of layer $(l+1)$. Equation (26) can be rearranged to give

$$\mathcal{D}^+_l = \mathcal{D}^+_{l+1} - K^+_l(\mathcal{D}^-_{l+1} - \mathcal{Q}^-_{l+1/2}) \qquad \text{where} \qquad K^+_l = \frac{\delta\tau_l}{\mu + \delta\tau_l/2}. \tag{27}$$

3.4 Convergence

The convergence of the algorithm is guaranteed under either of two simple conditions, as demonstrated by O'Brien (1992). The first occurs when the medium is absorbing, so that the single scattering albedo is bounded above by a number strictly less than one. The second arises when the optical thickness is finite. Because the application of the present code is to atmospheres containing only aerosol (and possibly thin cloud), the second condition is always satisfied. In practice, for optical thicknesses of around $\tau = 0.1$, about five iterations will be required. Acceleration techniques, such as those developed by O'Brien (1992), may be applied to improve efficiency. This option may be added in future versions of the code.

In practice, the iterations are terminated when successive estimates of the largest component of the upward scattered flux density at the top of the atmosphere differ by less than a specified tolerance, typically set at 10^{-4}.

3.5 Numerical integrations (quadratures)

At every stage of the iterative solution, the diffuse radiance must be integrated over solid angle to compute the source function $\mathcal{Q}$. The integrations are performed using gaussian quadrature for the zenith integration over $\mu = \cos\theta$ and trapezoidal quadrature for the azimuth integration over φ. The choices are self-evident: gaussian quadrature of degree N is exact for polynomials of degree up to $2N-1$, whereas trapezoidal quadrature with m points is $O(m^{-k})$ for integration of periodic functions with continuous k^{th} derivatives.

The upper and lower hemispheres are denoted by Ω^+ and Ω^-, so it is desirable to adopt a similar convention for labelling the zenith angles as follows.

1. Without any loss of generality, the degree N of the gaussian quadrature rule is required to be even, $N = 2n$. The quadrature points lie in the range $(-1, 1)$, with half in $(-1, 0)$ and half in $(0, 1)$. The points with negative μ are indexed by $-n, \ldots, -1$, and the points with positive μ by $1, \ldots, n$. In addition, a dummy quadrature point is introduced at $\mu_0 = 0$ with weight $w^\mu_0 = 0$. Thus, the complete set of quadrature points is

   $$-1 < \mu_{-n} < \cdots < \mu_{-1} < \mu_0 = 0 < \mu_1 < \cdots < \mu_n < 1$$

   with corresponding gaussian weights $w^\mu_{-n}, \ldots, w^\mu_n$.

2. The m points chosen for the trapezoidal quadrature are equally spaced in azimuth, with
$$0 = \varphi_0 < \varphi_1 < \cdots < \varphi_{m-1} < 2\pi.$$
The weights associated with the quadrature points are
$$w_j^{\varphi} = \frac{1}{2\pi} \begin{cases} \pi/m, & j = 0, \\ 2\pi/m, & j = 1, \ldots, m-2, \\ \pi/m, & j = m-1. \end{cases}$$

3. For each combination (μ_i, φ_j), define a unit vector $\mathbf{s}_{ji}$ with zenith angle θ_i (corresponding to μ_i) and azimuth φ_j via
$$\mathbf{s}_{ji} = \begin{pmatrix} \sin\theta_i \cos\varphi_j \\ \sin\theta_i \sin\varphi_j \\ \cos\theta_i \end{pmatrix}.$$

With these definitions, vector $\mathbf{s}_{ji}$ lies in the upper hemisphere Ω^+ when $i > 0$, and in the lower hemisphere Ω^- when $i < 0$.

Integration over solid angle is replaced by quadrature,
$$\int_{\Omega} d\omega(\mathbf{s})\, f(\mathbf{s}) \approx \sum_{i=-n}^{n} \sum_{j=0}^{m-1} w_{ji} f(\mathbf{s}_{ji}),$$
where the weights are given by
$$w_{ji} = w_j^{\varphi} w_i^{\mu}.$$
Calculation of these integrals is the most costly component of the algorithm.

4 Coding issues

4.1 Storage and rotational symmetry

The allocation of scattering matrices for all layers, all species, and all inward and outward directions leads to huge arrays. Consider, for example, the (a, b) element of the scattering matrix, $P_{ab}(\tau_{l-1/2}, \theta_i, \varphi_j, \theta_{i'}, \varphi_{j'})$ with 10 layers, 40 zenith angles, 20 azimuths and 8 bytes per element. The number of bytes required per species would be
$$\underset{\text{bytes}}{8} \times \underset{a}{4} \times \underset{b}{4} \times \underset{\text{layers}}{10} \times \underset{\theta_i}{40} \times \underset{\varphi_j}{20} \times \underset{\theta_{i'}}{40} \times \underset{\varphi_{j'}}{20} = 2^{13} \times 10^5 = 800\,\text{MB}.$$

Although computers with a gigabyte of memory are now commonplace, the numerical cost to fill the arrays would make the code unwieldy and slow. Therefore, simplifications are needed, and fortunately many are possible. Options include the following.

1. Use only four bytes per element.

2. Generally P_{ab} has only ten independent elements, rather than sixteen. Furthermore, for most applications with natural sunlight, the circular polarization component (expressed by the V component of Stokes' vectors) may be set to zero, leading to Stokes' vectors with only three components and scattering matrices with at most nine components.

3. The scattering matrix for molecules does not depend upon height.

4. Although aerosol properties vary with height, often the profiles will be known only poorly, so it may be reasonable to assume that the aerosol scattering matrix is independent of height.

5. In many cases the medium will possess symmetries, so not all elements need be stored.

The last offers a large reduction in storage for the case where the medium is invariant under rotations about the vertical axis. Because this situation includes all the applications of immediate interest, we will assume this symmetry and adopt a storage strategy accordingly. However, it must be remembered that the assumption is invalid for surfaces with a preferred direction, such as dunefields.

Assume that Ω, the domain of integration, is invariant under rotations about the z-axis. In practice the only cases that will arise will be the full sphere and the upper and lower hemispheres. Thus, if R denotes a rotation about the z-axis, then

$$R\Omega = \Omega \qquad \text{and} \qquad d\omega(R\mathbf{s}) = d\omega(\mathbf{s}), \tag{28}$$

expressing the invariance of both Ω and the solid angle measure.

$P(\mathbf{s}, \mathbf{s}')$ denotes the probability of scattering from $\mathbf{s}'$ to $\mathbf{s}$ (with associated polarization changes). P is defined so that the reference plane for incident radiation is defined by $\mathbf{n}$ and $\mathbf{s}'$, while that for scattered radiation is defined by $\mathbf{n}$ and $\mathbf{s}$. If the medium is invariant under rotations about $\mathbf{n}$, then

$$P(\mathbf{s}, \mathbf{s}') = P(R\mathbf{s}, R\mathbf{s}') \tag{29}$$

for any rotation R about $\mathbf{n}$. (Think of the ray directions as fixed, and rotate the medium underneath. If the physical results are the same, as they will be for a medium invariant under such rotations, then condition (29) is satisfied.)

Now consider an integral of the form

$$\mathcal{B}(\mathbf{s}) = \int_{\Omega} d\omega(\mathbf{s}')\, P(\mathbf{s}, \mathbf{s}')\mathcal{A}(\mathbf{s}'),$$

where $\mathcal{A}$ represents any Stokes' vector, and consider the effect of a rotation R on $\mathbf{s}$,

$$\mathcal{B}(R\mathbf{s}) = \int_{\Omega} d\omega(\mathbf{s}')\, P(R\mathbf{s}, \mathbf{s}')\mathcal{A}(\mathbf{s}'). \tag{30}$$

Let

$$\mathbf{s}' = R\mathbf{s}''$$

and transform equation (30) as follows:

$$\begin{aligned}
\mathcal{B}(R\mathbf{s}) &= \int_{\Omega} d\omega(R\mathbf{s}'')\, P(R\mathbf{s}, R\mathbf{s}'')\mathcal{A}(R\mathbf{s}'') \\
&= \int_{R^{-1}\Omega} d\omega(\mathbf{s}'')\, P(\mathbf{s}, \mathbf{s}'')\mathcal{A}(R\mathbf{s}'') \\
&= \int_{\Omega} d\omega(\mathbf{s}')\, P(\mathbf{s}, \mathbf{s}')\mathcal{A}(R\mathbf{s}'),
\end{aligned} \tag{31}$$

where the invariance properties of Ω and P expressed in equations (28) and (29) have been used. Equation (31) shows that the rotation applied to the argument of $\mathcal{B}$ may be transferred to the Stokes' vector $\mathcal{A}$ in the integrand.

This result is important because the unit vector $\mathbf{s}_{ji}$ corresponding to zenith angle θ_i and azimuth φ_j can be generated from the vector $\mathbf{s}_{0i}$ with azimuth zero by a rotation R_j about the z-axis,

$$\mathbf{s}_{ji} = R_j \mathbf{s}_{0i}.$$

Thus, the value of $\mathcal{B}$ for any direction $\mathbf{s}_{ji}$ may be written in the form

$$\mathcal{B}(\mathbf{s}_{ji}) = \mathcal{B}(R_j \mathbf{s}_{0i}) = \int_{\Omega} d\omega(\mathbf{s}')\, P(\mathbf{s}_{0i}, \mathbf{s}') \mathcal{A}(R_j \mathbf{s}'),$$

which reduces to the quadrature

$$\mathcal{B}(\mathbf{s}_{ji}) = \sum_{i'=-n}^{n} \sum_{j'=0}^{m-1} w_{j'i'} P(\mathbf{s}_{0i}, \mathbf{s}_{j'i'}) \mathcal{A}(R_j \mathbf{s}_{j'i'}). \tag{32}$$

Because

$$R_j \mathbf{s}_{j'i'} = \mathbf{s}_{k'i'},$$

where the index k' is given in terms of j and j' by

$$k' = (j + j') \mod m,$$

equation (32) gives

$$\mathcal{B}(\mathbf{s}_{ji}) = \sum_{i'=-n}^{n} \sum_{j'=0}^{m-1} w_{j'i'} P(\mathbf{s}_{0i}, \mathbf{s}_{j'i'}) \mathcal{A}(\mathbf{s}_{k'i'}),$$

which shows that it is only necessary to evaluate P for exit rays with zero azimuth in order to compute $\mathcal{B}$ for *any* direction. If $\mathcal{A}$ is stored with rows labelled by azimuth index j and columns labelled by zenith index i,

$$\begin{array}{cc} & \begin{array}{ccc} & i & \\ -n & \ldots\ldots & n \end{array} \\ \begin{array}{c} \\ j \\ \\ \end{array} & \begin{array}{c} 0 \\ \vdots \\ m-1 \end{array} \left(\begin{array}{ccc} & & \\ & \mathcal{A}_{ji} & \\ & & \end{array} \right) \end{array}$$

then the matrix $\mathcal{A}_{k'i'}$ is obtained from $\mathcal{A}_{j'i'}$ by cyclically shifting each column upwards by j places. The process can be carried out elegantly in Fortran 95 by

$$\mathsf{A} = \mathsf{CSHIFT(A,J)}$$

Thus, if Domain denotes a logical array that selects the full sphere, the upper hemisphere or the lower hemisphere of rays, then the code to evaluate $\mathcal{B}(\mathbf{s}_{ji})$ for all $\mathbf{s}_{ji}$ reduces to the following few lines:

```
DO I=−N,N
    DO J=0,M−1
        WHERE (Domain)
            Q=QuadWeight∗ScatMatrix(I,:,:)∗A
        END WHERE
        A=CSHIFT(A,1)
        B(J,I)=SUM(Q,Mask=Domain)
    END DO
END DO
```

The scattering matrix is ScatMatrix(I,J',I'), corresponding to $P(\mathbf{s}_{0i}, \mathbf{s}_{j'i'})$. This strategy leads to very neat code and effects an m-fold reduction in the storage required for the scattering matrices.

4.2 Subroutine Radiation

The most difficult part of any radiation code (illustrated by the flow chart in figure 1) is that of defining the atmospheric structure and performing the spectral integrations, whether over broad bands to calculate fluxes and atmospheric heating as in general circulation models or over the relatively narrow bands of satellite radiometers for remote sensing applications. Therefore, it makes good sense to structure the code so that supervision of the tasks of defining the atmospheric environment and integrating over frequency are decoupled from the details of the algorithm by which the RTE is solved. Achieving this logical separation requires considerable care in defining the structures for input and output data, but the benefits in clarity, ease of maintenance and portability of the code far outweigh the cost incurred in careful planning. In order to illustrate these principles, we give here an outline of subroutine Radiation that lies at the core of the radiation code. Although neither the largest nor the most complex subroutine, it provides a good example of the issues raised above. The objective is to have modular code that allows alternative algorithms for solving the monochromatic RTE to be plugged into a well-defined interface without requiring modification of the spectral integration modules.

Subroutine Radiation has two arguments, Photon and Radiance, the first providing the data for the calculation and the second conveying the results. Photon is a variable of type Photon_Data, a structure with many components specifying the layers and levels of the atmosphere, the scattering geometry, the gaseous and particulate composition, the optical properties, and the spectral bands used for the computation. Radiance, on the other hand, is a variable of type Radiance_Data, which defines the output quantities. Even though subroutine Radiation supervises the calculation of Radiance, it never needs to know exactly what Radiance_Data is. That information is confined to a separate module called RTE_Solver_Module, where Radiance_Data is defined along with the procedures that manipulate Radiance_Data.

There will be several instances of RTE_Solver_Module. For example, one version defines Radiance_Data to be flux densities at layer interfaces, and computes Radiance using a two-stream approximation. Such a version has application to calculating atmospheric heating rates for dynamical models of the atmosphere. A second version, the subject of this report, defines Radiance_Data to be the complete polarized radiance field, and solves the RTE with the iterative algorithm defined in earlier sections. In each case, the structure Radiance_Data

will include a further structure defining Optics_Data, which may vary between instances of RTE_Solver_Module.

Data for subroutine Radiation provided in Photon include a distribution of specific absorption for each of the absorbing species in each of the frequency bands. The distributions are correlated, in the sense defined by Goody et al. (1989) and Lacis and Oinas (1991), and they provide an efficient and accurate approximation for calculating spectral properties, as demonstrated by O'Brien and Dilley (2000). In the literature such distributions usually are called 'correlated k-distributions', because k often is used to denote specific absorption, but here we will use the acronym CDSA, standing for correlated distribution of specific absorption. The CDSA for each gas is computed on a pressure and temperature grid (p, T) that is specific to the gas. Although in simple situations a common grid may be used for all gases, usually the grids are tailored to the vertical distribution and strength of the absorption. The CDSAs are precomputed, a task that is numerically intensive and requires gigabytes of temporary storage, but ultimately leads to tabulations that are small and manageable.

The steps of subroutine Radiation, shown in figure 8, are as follows.

1. In preparation for interpolating the CDSA for each gas from the (p, T) grid used in the tabulation to the (p, T) grid of the atmosphere, each atmospheric (p, T) is located within the tabulation grid and the indices of the cell containing (p, T), as well as the increments into the cell, are stored for subsequent use. These indices and increments may change with every call to Radiation if the atmosphere is evolving dynamically or thermodynamically.

2. The optical properties of aerosol, cloud and continuum are computed for each band. Because the properties are assumed to vary slowly (the 'grey body' approximation), only one calculation is required for each band.

3. The CDSA is computed at the atmospheric (p, T) grid for each gas by interpolation in the tables of precomputed CDSAs, and the distributions for the individual gases are combined in an optimized way to produce a CDSA for the mixture of gases.

4. The algorithm then begins an inner loop over points in the CDSA.

   (a) For each point, the specific absorption and specific scattering by gases are computed for all layers, leading to a complete specification of the optical properties of the atmosphere.

   (b) The call to the RTE solver is split into two stages, an initial call to define parameters of the algorithm and a subsequent call to compute the radiance. The reason for the split is to allow Set_RTE_Solver_Parameters to perform preliminary calculations using structures not known to subroutine Radiation. For example, in the polarized code, subroutine Radiation does not know the definition of either Radiance_Data or Optics_Data, some elements of which may not be defined by the time subroutine Radiation is ready to call subroutine RTE_Solver. The preliminary call to subroutine Set_RTE_Solver_Parameters addresses this problem by providing an opportunity to complete the specification of the radiative transfer problem.

   (c) The radiance returned by the RTE solver is assigned a weight (determined by the CDSA) and added to the total radiance.

Subroutine Radiation returns the radiance for each band and also the cumulative radiance over all bands. In order to effect these calculations, subroutine Radiance needs only elementary operations such as Add_Radiance, the details of which are delegated to the RTE_Solver_Module. Thus, with careful definition of the structures and allocation of the responsibility to manipulate structures, the tasks of defining the atmospheric environment and integrating over frequency may be separated from the more specific task of solving the monochromatic RTE.

The rest of this section describes some of the structures used by the polarized version of RTE_Solver_Module to achieve these objectives.

4.3 Structures used by subroutine Radiation

This subsection describes briefly the key data structures used by subroutine Radiation. The description is not intended to be exhaustive, but nevertheless should be sufficient to allow a competent programmer to follow the code.

4.3.1 Type Radiance_Data

The elements of type Radiance_Data are shown in figure 9. Most of the names are self explanatory, but a few comments may help.

If NumComponents is set to unity, then the code reverts to an unpolarized radiation code and computes only the unpolarized intensity, but all components of the Stokes' vector for the polarized radiance will be computed if NumComponents is set to four.

Stokes' vector RSca represents the diffuse (scattered) radiance $\mathcal{D}$ defined in section 2. RSca is declared as a pointer with unspecified length. Allocation of the array occurs in subroutine Allocate_Radiance, where the dimension is set to the number of levels, indexed from 0 to NumLayers. Similarly, Stokes' vectors RDir and RTot represent the solar radiance $\mathcal{I}_\star$ and the total radiance $\mathcal{I} = \mathcal{I}_\star + \mathcal{D}$, with 'Dir' and 'Tot' referring to 'direct' and 'total'.

FScaUp and FScaDown denote the upward and downward diffuse (scattered) flux densities at the top of the atmosphere and at the surface, respectively. The arrays are allocated in subroutine Allocate_Radiance with dimension NumComponents. Flux densities are not reported for the intermediate levels of the atmosphere.

Polarization represents the (positive) polarization

$$P = \sqrt{Q^2 + U^2 + V^2}/I,$$

whereas RubensonPolarization represents the (possibly negative) quantity

$$P_R = Q/I.$$

Both Polarization and RubensonPolarization are defined at all levels, indexed by 0 to NumLayers.

4.3.2 Type Stokes_Vector

Variables of type Stokes_Vector (figure 10) are vectors with length NumComponents, so the radiance is either unpolarized or polarized depending upon whether NumComponents is equal to 1 or 4. Each element of the array has type Stokes_Vector_Table, defined to be a two-dimensional array (figure 11). The first index, $j = 0, \ldots, m-1$, labels the azimuth, while the second index, $i = -n, \ldots, n$, labels the zenith angle of the direction of propagation of the photons. Thus, with RSca as an example,

$$\mathsf{Radiance\%RSca(L)\%Vector(A)\%Table(J,I)}$$

denotes the diffuse radiance $\mathcal{D}_a(\tau_l, \mu_i, \varphi_j)$. The use of structures in this way is the key to enforcing the 'need to know' principle. Subprograms may manipulate the higher level structures without knowing even the existence of lower levels. In contrast, if (following the conventions of Fortran 77) RSca is declared as a four-dimensional array indexed by L, A, I and J, then any subprogram to which it is passed will inherit the baggage associated with all the dimensions, including those that are not needed for the calculation in hand.

4.3.3 Type Phase_Matrix

Scattering matrices are represented as variables with type Phase_Matrix (defined in figure 12). At the top level, a variable of type Phase_Matrix is a square matrix with dimension NumComponents, each element of which has type Phase_Matrix_Table. The latter, defined in figure 13, has two components.

1. Table is a three-dimensional array whose first index i labels the zenith angle of the exit direction $\mathbf{s}_{0i}$, while the second and third indices, j' and i', label the azimuth and zenith angle of the incident direction $\mathbf{s}_{j'i'}$.

2. TableSun is a two-dimensional array whose indices, j and i, label the azimuth and zenith angle of the exit direction $\mathbf{s}_{ji}$ for photons scattered from the incident direction defined by the solar beam.

As an example, consider the component Phase of the type Optics_Data (defined below). Phase is a pointer with dimension equation to NumLayers, every element of which has type Phase_Matrix. Thus,

$$\mathsf{Phase(L)\%Matrix(A,B)\%Table(I,JPrimed,IPrimed)}$$

denotes the (a, b) element of the scattering matrix at the mid-point of layer l,

$$P_{ab}(\tau_{l-1/2}, \mu_i, \varphi_0, \mu_{i'}, \varphi_{j'}),$$

while

$$\mathsf{Phase(L)\%Matrix(A,B)\%TableSun(J,I)}$$

denotes the corresponding element evaluated with the direction of the solar beam, specified by $\mu_\star = \cos\theta_\star$ and $\varphi_\star$, as the incident direction,

$$P_{ab}(\tau_{l-1/2}, \mu_i, \varphi_j, \mu_\star, \varphi_\star).$$

4.3.4 Type Optics_Data

Figure 14 shows the components of the structure Optics_Data that contains the essential optics data required by the code. Arrays AbsOT, ScaOT and ExtOT are allocated with size NumLayers, and are used to store the absorption, scattering and extinction optical thicknesses of the layers. Albedo stores the single scattering albedo. It is redundant in principle, because the albedo may be computed from the scattering and extinction optical thicknesses (assuming optical properties are constant in the layer), but nevertheless is useful in practice. Phase contains the scattering matrix, as described above.

The variable NumLayersPhase requires special comment. The scattering matrix must be defined for every layer, but for some species (such as molecules), the form of the scattering matrix is independent of number density and hence height. In such cases, NumLayersPhase is set to unity rather than NumLayers, and the code uses the scattering matrix defined for the first layer for all other layers. This device saves storage and time, because the time required to fill the scattering matrices is considerable.

5 Test cases

5.1 Introduction

Three sources of test data have been used. Azimuthally integrated unpolarized radiance has been tabulated by van de Hulst (1980) for uniform layers with scattering determined by either the isotropic phase function or the Henyey-Greenstein phase function (Henyey and Greenstein, 1941). These tables are useful only for isotropic scattering, for which the radiance is azimuthally symmetric. The Monte Carlo algorithms of O'Brien (1992, 1998) provide highly accurate radiances for arbitrary geometry, but again are limited (presently) to unpolarized radiances. Probably the most comprehensive set of tabulations of polarized radiances are for the Rayleigh atmosphere, with and without a reflecting lower boundary, published by Coulson et al. (1960). The latter were taken as the principal source for comparisons.

Reported here are the results of three test cases encompassing roughly the range of situations anticipated in practice:

1. a Rayleigh atmosphere with optical thickness $\tau = 0.1$ lying above a black surface;
2. a Rayleigh atmosphere with $\tau = 1$ lying above a Lambert surface with albedo 0.25;
3. a composite atmosphere containing both molecules and aerosol (the properties of which will be described later) lying above a Lambert surface with albedo 0.25.

Testing of the code involves two issues. The first, rather esoteric, is that of 'correctness' of the code, by which is meant that the error in any calculated radiance can be reduced to the level set by the precision of the computer hardware if sufficient computing power is expended. The second issue, more important in practice, concerns the rate of convergence, because this information is needed in the delicate balance between accuracy and cost. To address the correctness issue, the scattered intensity seen in the direction of the sun by an observer on the ground is compared with the results tabulated by Coulson et al. (1960) in tables 1 and 2. This geometrical configuration provides the most difficult comparison, because the radiance varies most rapidly across the solar aureole. Generally the agreement of the most refined calculation with the tables is within the accuracy of the tables (reckoned to be ± 2 in the fifth decimal place outside the solar aureole, and somewhat larger within). Thus, the correctness of the code seems assured.

To investigate the rate of convergence, radiances computed with a highly refined discretization were taken as 'truth' against which radiances computed with coarser discretizations were compared. The three variables that control the convergence of the algorithm are the number of levels (L) and the degrees (M and N) of the quadratures used for the azimuth and zenith angle integrations. For each of the test cases described above, experiments were conducted in which one of L, M and N was varied while the other two were held constant. The results are presented as a series of plots showing the convergence of the intensity and degree of polarization at the surface and the top of the atmosphere as functions of the zenith angle.

For the test cases involving only Rayleigh scattering, it is known theoretically that the diffuse radiance, when expanded in Fourier series in the azimuth φ, contains only the first three terms. Therefore, it follows from the sampling theorem (Bracewell, 1978) that any trapezoidal quadrature with six or more evenly spaced points will suffice to integrate the radiance over azimuth without error. Consequently, the convergence tests for the Rayleigh atmosphere were conducted with $M = 6$, and only L and N were varied. In contrast, the

third test case was used with L and N fixed, but M was varied to check the convergence as the azimuth integration was refined.

A secondary, but very practical issue, that arises in these comparisons concerns the gaussian quadrature points used for the zenith angle integrations. The point sets corresponding to different degree quadrature rules are disjoint, so comparison of radiances computed with quadratures with different degrees is possible only if the radiances are interpolated to a common grid. This interpolation is itself a source of error, but should be regarded as an integral part of computing radiances. Only rarely will applications require radiances at gaussian quadrature points! There are many candidates for the interpolation, but none is entirely satisfactory.

1. Linear interpolation fails to represent the functions well in regions of rapid change if the gaussian points are widely spaced.

2. Polynomial interpolation, for example with Legendre polynomials, is numerically unstable for polynomials with high degree. Thus, fidelity in reproducing the data leads inevitably to unrealistic oscillations between the data points. The problem may be alleviated by limiting the order of the polynomial and determining the coefficients to minimize the residual sum of squares, but the penalty is reduced accuracy at the tabulation points. Interpolation polynomials with different degrees can differ markedly.

3. Cubic splines with gradients specified at the end points appear preferable to Legendre polynomials, but specification of the gradient is problematic. Linear interpolation from the last two points performs poorly when the function is changing rapidly near the end points. Quadratic interpolation of the gradient from the last three points can introduce unacceptable oscillations, although these are localized near the end points.

The option selected for the tests of this report was to use a natural spline, determined uniquely by the data points and the requirement that the second derivative should vanish at the end points. Although this approach appears to be satisfactory most of the time, it is responsible for some of the oscillatory behaviour apparent near the end points in the error plots that follow.

5.2 Rayleigh atmosphere, $\tau = 0.1$, $A = 0$

5.2.1 Intensity

Figure 15 shows the intensity (normalized by the solar flux density) for the test case with a Rayleigh scattering atmosphere with optical thickness $\tau = 0.1$ over a black surface. The solar zenith angle in figure 15 and all subsequent plots is fixed at $\theta_\star = 113.58°$, so that

$$\mu_\star = \cos\theta_\star = -0.4,$$

corresponding to one of the test configurations tabulated by Coulson et al. (1960). The figure has six panels; the rows indicate the value of the intensity, its absolute error ($\times 100$) and its relative error, while the left- and right-hand columns represent the downward intensity at the surface and the upward intensity at the top of the atmosphere (TOA). The relative azimuth of sun and observer is $\varphi = 0°$, so the scattering is in the principal plane. Thus, at both the surface and the TOA, the intensities are those seen by an observer looking into the sunward hemisphere. The several curves in each panel correspond to

different values of N, the degree of the gaussian quadrature used for the zenith angle integration. The error plots have one fewer curve, because the calculation with the most refined discretization from the upper row has been used as the reference for calculating errors.

The upper row shows that the intensity converges well at both the surface and the TOA. The scattered intensity is similar in form at the surface and the TOA, because the surface is non-reflecting and the atmosphere is thin. In both cases, the intensity rises towards the horizon because the path along which scattering occurs lengthens. The error plots exhibit a feature that is common to many of the plots, that the errors in intensity are concentrated in a band of zenith angles that migrates towards the horizon as the degree of the quadrature is increased. Furthermore, the maximum amplitude of the error in the band remains approximately constant, no matter what the degree of the quadrature rule. As a very rough guide, to achieve an accuracy of a few percent in the range

$$\hat{\mu} \leq \mu \leq 1,$$

then the degree of the quadrature rule needs to be approximately

$$N \approx 8/\hat{\mu}.$$

Figure 16, identical in form to figure 15, applies to the intensity scattered with azimuth $\varphi = 60^\circ$ relative to the sun. The scattered intensity is lower than in the principal plane, because the scattering angle is closer to the value for which the unpolarized scattering phase function has a minimum. The conclusions regarding errors are similar to figure 15.

The sensitivity of the scattered intensity to the vertical discretization is explored in figure 17, again with six panels similar in form to figure 15. In this test case the total optical thickness is $\tau_L = 0.1$, and figure 17 shows intensities computed with subdivision of the atmosphere into 1, 2, 5 and 10 layers of equal thickness. The differences are very small, except when viewing towards the horizon. The reason is clear. Although the vertical optical thickness τ_L of the atmosphere is small, rays at zenith angle θ see path length $\tau_L/\cos\theta$ between the surface and space, so the replacement of $\partial/\partial\tau$ by a finite difference is liable to significant error for such rays. The behaviour in figure 18 for azimuth $\varphi = 60^\circ$ is similar. As a very rough guide, the ratio $\delta\tau/\hat{\mu}$ should not exceed about 1/2 if intensities accurate to a few percent are required in the range $\hat{\mu} \leq \mu \leq 1$.

5.2.2 Polarization

The polarization of scattered radiance at the surface and the TOA, along with the associated absolute and relative errors, are shown in figures 19 and 20, the former corresponding to scattering with azimuth $\varphi = 0^\circ$ and the latter with $\varphi = 60^\circ$.

At the TOA, the maximum polarization in the principal plane occurs near $\mu = 0.92$, where its value is over 90%. Under this configuration, the scattering angle is 90°, and the radiation would be perfectly polarized if only single scattering were occurring. The degree of depolarization is an indication of the extent of multiple scattering, and is small for the case of an optically thin atmosphere. The errors oscillate near zenith, an effect almost certainly caused by the interpolation procedure. Near the horizon the absolute error remains constant, but the relative error rises because the degree of polarization is falling.

For scattering with azimuth $\varphi = 60^\circ$, as shown in figure 20, the degree of polarization at the TOA remains relatively high over the full range of view angles, principally because the range of scattering angles is narrower than in the case of the principal plane. The

absolute errors are comparable with those for the principal plane, but the relative errors are smaller simply because the radiation is more highly polarized.

The situation at the surface is more complex because there are two 'neutral' points where the polarization is zero. The positions of the neutral points are sensitive indicators of both the amount and the type of atmospheric turbidity. The neutral point closer to zenith is the 'Babinet point', while the point closer to the horizon is the 'Brewster point', named after the French meteorologist and Scottish physicist who discovered them in 1840 and 1842. Although the absolute errors remain small, the relative errors become huge near the neutral points. Fortunately, a large relative error in a negligibly small quantity has no physical significance.

Neutral points occur only when Q, U and V vanish simultaneously. For a Rayleigh atmosphere, V is always zero if the incident radiation is unpolarized, and U vanishes in the principal plane, so neutral points will occur whenever Q also is zero in the principal plane. In other planes, however, U is not identically zero, so circumstances causing neutral points are rare. Therefore, it is not surprising that figure 20 with azimuth $\varphi = 60°$ does not show neutral points. The polarization varies slowly with a minimum near $\mu \approx -0.7$, corresponding to $\theta \approx 45°$. The errors generally are small, but increase towards the horizon.

The sensitivity of the polarization to the vertical discretization is shown in figures 21 and 22. In the principal plane, the absolute errors remain small at both the surface and the TOA. However, the relative error at the surface is large near the neutral points, while at the TOA it increases towards the horizon, because the polarization decreases there. At an azimuth of $\varphi = 60°$, the relative errors are less than 1% for all discretizations considered. This is in contrast to the intensity, which exhibits large variations near the horizon. Presumably the discretization affects all components of the Stokes' vector similarly, so that some cancellation of errors occurs in the calculation of the polarization.

5.3 Rayleigh atmosphere, $\tau = 1$, $A = 0.25$

5.3.1 Intensity

In this test case, which has moderate optical thickness and surface albedo, the scattered intensities at the surface and at the TOA are no longer similar in form. As shown in figure 23 for the principal plane, the intensity at the surface has a broad maximum near the solar direction, caused by the bias towards forward rather than sideways scattering in the Rayleigh scattering matrix. At the TOA, the intensity is larger than at the surface because it has a significant contribution from surface reflection. The maximum occurs at zenith, where the path length for reflected rays is least, and decreases towards the horizon, where it is roughly comparable with the horizon intensity at the surface.

The errors do not increase so systematically towards the horizon as with the thin Rayleigh atmosphere in the previous example. The reason probably lies in the interpolation procedure. For the thin atmosphere over a black surface, the intensity rose rapidly near the horizon, and spline approximation between the gaussian quadrature points introduces systematic errors. For the thicker atmosphere, where multiple scattering dominates, the intensity varies less rapidly with angle and the interpolation errors are smaller. In general, however, the errors are small for all the quadrature rules considered.

The situation shown in figure 24 for scattering with azimuth $\varphi = 60°$ is similar to that shown in figure 23 for the principal plane. This is not surprising, because multiple scattering smooths out the dependence upon viewing geometry.

The sensitivity of the intensity to the vertical discretization is shown in figures 25 and 26 for azimuths $\varphi = 0°$ and $\varphi = 60°$. Both show that large errors occur near the

horizon if the vertical discretization is too coarse. The reasons given in the discussion of the thin atmosphere apply equally here, as does the rule of thumb for estimating the maximum layer thickness $\delta\tau$ permissible if a specified accuracy is to be achieved.

5.3.2 Polarization

Figure 27 shows the polarization in the principal plane. Compared with the case for the thin atmosphere, there are two significant differences. Firstly, the degree of polarization is much lower, indicating that multiple scattering dominates over single scattering. Secondly, the Brewster point is below the horizon and the Babinet point has shifted closer to the zenith. This is consistent with the results of Coulson (1954) (reported in more accessible form by Coulson (1988)) that the angular distances of the Babinet and Brewster points from the sun generally increase with optical thickness.

The absolute error in the polarization in the principal plane at the surface is large in the neighbourhood of the Babinet point. This may be an artifact of the interpolation, because the polarization varies most rapidly near the Babinet point. Similarly, at the TOA the maximum polarization occurs near zenith, and interpolation near the maximum may be the cause of the oscillations in the absolute error. The relative errors are large whever the polarization is small, most obviously near the Babinet point at the surface and near the horizon at the TOA.

For scattering with azimuth $\varphi = 60^\circ$, the prominent minimum in the surface polarization shown in figure 20 for the thin atmosphere is reduced to a shallow depression for the present case, shown in figure 28. Furthermore, the minimum has migrated towards the horizon. The relative errors generally are very small, but rise to about 1% in regions where the polarization is varying most rapidly.

Finally, the sensitivity of the polarization to the vertical discretization is shown in figures 29 and 30 for scattering azimuths $\varphi = 0^\circ$ and $\varphi = 60^\circ$. The polarization at the TOA is computed accurately for all discretizations shown, but the surface polarization computed with $\delta\tau = 0.2$ exhibits large errors for $\mu < 0.1$, again supporting the conclusion that, in order to achieve accuracy in the range $\hat{\mu} \le \mu \le 1$, one should require $\delta\tau/\hat{\mu} \approx 1/2$.

5.4 Molecular and aerosol atmosphere, $\tau = 0.2$, $A = 0.25$

The atmosphere for this test case is assumed to have an optical thickness $\tau_m = 0.1$ due to molecules and $\tau_a = 0.1$ due to aerosol. The aerosol particles are assumed to have sizes distributed according to the power law

$$n(r) = \frac{2r_-^2 r_+^2}{r_+^2 - r_-^2} r^{-3}, \qquad r_- \le r \le r_+,$$

where r_- and r_+ are the lower and upper limits of the size distribution. The effective radius and effective variance are given in terms of $r_\pm$ by

$$r_{\text{eff}} = \frac{r_+ - r_-}{\ln(r_+/r_-)} \qquad \text{and} \qquad v_{\text{eff}} = \frac{r_+ + r_-}{2(r_+ - r_-)} \ln(r_+/r_-) - 1.$$

This specific choice for the size distribution is not as restrictive as it might at first appear, because Hansen and Travis (1974) and Mischenko and Travis (1994) have shown that any two monomodal distributions with the same effective radius and effective variance lead to almost identical scattered radiances. For the test, the effective radius was chosen to be $r_{\text{eff}} = 0.5\,\mu\text{m}$, with (dimensionless) effective variance $v_{\text{eff}} = 0.25$, corrresponding approximately with the distributions observed by O'Brien et al. (1999) at Tinga Tingana

in the Strzelecki Desert of South Australia. The limits of the size distribution, obtained using the iterative procedure described by Mischenko and Travis (1994), are

$$r_- = 0.181\,\mu\text{m} \qquad \text{and} \qquad r_+ = 1.069\,\mu\text{m}.$$

The wavelength was assumed to be 500 nm, and the particles were assumed to be spherical with refractive index $1.54 - 0.01i$. A Mie calculation returned the aerosol single scattering albedo $\varpi_a = 0.903$, asymmetry parameter $g = 0.705$ and scattering functions, from which the scattering matrix was constructed. The unpolarized phase function, shown in figure 31, has a sharp forward peak, a characteristic minimum for sideways scattering, and a much smaller peak for retro-scattering. The coefficients of the expansion of the scattering function M_1 are shown in figure 32.

5.4.1 Intensity

Table 3 presents a spot check on the convergence of the scattered intensity as the degree of the azimuth quadrature and the number of levels are increased. As with the other tables and plots, the solar zenith angle $\theta_\star$ is fixed so that $\mu_\star = \cos\theta_\star = -0.4$, corresponding with one of the test cases listed by Coulson et al. (1960). The table shows that the convergence is rapid, requiring 8 iterations, $L = 5$ layers and quadrature rules with $M = 24$ and $N = 20$ terms to achieve convergence to better than three significant figures.

The convergence of the intensity as the azimuth integration is refined is shown in figure 33 for the principal plane. The scattered intensity at the surface has a sharp peak near the direction of the solar beam. Comparison with figure 15 shows the huge impact of a moderate amount of aerosol on the solar aureole, caused by the strong forward scattering by aerosol. Note that the peak is shifted from the direction of the solar beam slightly towards the zenith, a consequence of the differential in path length for rays scattered above and below the sun. At the TOA the intensity is higher than in figure 15, principally because the surface is reflecting. The effect of aerosol upon intensity reflected to space may be either positive or negative, depending upon the brightness of the surface and the optical thickness of the aerosol, because scattering by aerosol, which brightens the scene, may be outweighed by attenuation by aerosol of the intensity reflected from the surface.

The convergence is relatively rapid. With $M = 12$ terms in the azimuth integration, the relative errors at the surface and the TOA are approximately 5%, but the errors diminish rapidly once the number of terms is increased to $M = 24$ and beyond. As a guide to the number of terms required, one can examine the coefficients of the expansion of the Mie scattering functions in Legendre series, as shown in figure 32 for the function M_1. The coefficients have fallen to 5% of the maximum within 12 terms, which suggests through the sampling theorem (Bracewell, 1978) that 24 terms should secure accuracy of 5% or better.

5.4.2 Polarization

The polarization in the principal plane shown in figure 34 differs in several interesting ways from that given earlier (figure 19) for a molecular atmosphere with $\tau = 0.1$ over a black surface. Firstly, the degree of polarization is much lower, primarily a consequence of unpolarized reflectance from the Lambert surface. The reduction is most noticeable in the direction of the solar beam, where the radiance is now almost completely unpolarized. Similarly, the polarization is low at the TOA, because the radiance reflected from the surface is unpolarized.

The convergence with increasing degree of the azimuth quadrature is rapid, with good results obtained once $M = 24$. As with the intensity, the number of terms required can be estimated from the rate of decay of the coefficients of the expansions of the Mie scattering functions in Legendre series.

6 Cimel sun-photometers

The purpose of this brief section is to relate the radiances computed by the RTE solver to the polarized channels of Cimel sun-photometers. This relation suggests a simplified processing strategy.

The Cimel sun-photometers have three polarized channels at a wavelength of 870 nm. The physical arrangement of the filters is shown in figure 35. The filter wheel has three openings set 120° apart for the polarizing filters. The whole filter wheel is covered with a sheet of polarizing material, whose axis of maximum transmission is indicated by the aligned arrows. The collimator is positioned over the opening shown at the top of figure 35. As the wheel rotates and filters 0, 1 and 2 move into position over the detector, the axis of maximum transmission for filter k will be inclined at angle

$$\chi_k = 2\pi k/3$$

to the horizontal. The reference planes are indicated in figure 36. The Stokes' vectors $\mathcal{I}'$ and $\mathcal{I}$ representing the radiance incident upon and transmitted by the filter are related (in the absence of attenuation) by

$$\mathcal{I} = T(\chi)\mathcal{I}',$$

where

$$T(\chi) = \begin{pmatrix} 1 & \cos\chi & \sin\chi & 0 \\ \cos\chi & \cos^2\chi & \cos\chi\sin\chi & 0 \\ \sin\chi & \sin\chi\cos\chi & \sin^2\chi & 0 \\ 0 & 0 & 0 & 0 \end{pmatrix}$$

is the transmittance of the polarizing filter inclined at angle χ (Coulson, 1988).

Application of this filter to select the component of the radiance with its electric field vector oscillating horizontally leads to the result shown in figure 37 for the test atmosphere with both molecular and aerosol scattering and a reflecting lower boundary. The negative zenith angles correspond to observations in the back-scattering hemisphere. The large peak is the solar aureole, caused by aerosol scattering. The solid line is the corresponding result for an atmosphere with the same molecular optical thickness and the same surface albedo, but without aerosol. Because the Rayleigh component is symmetrical about the zenith, and because the aerosol contribution is very small in the back-scattering hemisphere, it may be possible to remove the Rayleigh contribution from the sun-photometer data simply by folding the back-scattering hemisphere to the forward-scattering hemisphere and subtracting. This process may avoid some of the difficult problems associated with calibration of the sky radiance channels of Cimel sun-photometers.

References

Bracewell, R. N., 1978: *The Fourier transform and its applications.* McGraw-Hill Kogakusha, Tokyo, second edition.

Chandrasekhar, S., 1950: *Radiative Transfer.* Oxford Univ. Press, Oxford.

Coulson, K. L., 1954: Neutral points of skylight polarization in a Rayleigh atmosphere. Sci. Rept. 7, Contr. AF19(122)-239, Univ. of California, Los Angeles.

Coulson, K. L., 1988: *Polarization and intensity of light in the atmosphere.* A. Deepak Publishing, Hampton, Virginia.

Coulson, K. L., J. V. Dave, and Z. Sekera, 1960: *Tables related to radiation emerging from a planetary atmosphere with Rayleigh scattering.* University of California Press, Berkeley & Los Angeles.

Deschamps, P.-Y., F.-M. Bréon, M. Leroy, A. Podaire, A. Bricaud, J.-C. Buriez, and G. Sèze, 1994: The POLDER mission: Instrument characteristics and scientific objectives. *IEEE Trans. Geosci. Remote Sens.*, **32**, 598–615.

Goody, R., R. West, L. Chen, and D. Crisp, 1989: The correlated-k method for radiation calculations in nonhomogeneous atmospheres. *J. Quant. Spectrosc. Radiat. Transfer*, **42**, 539–550.

Hansen, J. E., and L. D. Travis, 1974: Light scattering in planetary atmospheres. *Space Sci. Rev.*, **16**, 527–610.

Henyey, L. G., and J. L. Greenstein, 1941: *Astrophys. J.*, **93**, 76.

Lacis, A. A., and V. Oinas, 1991: A description of the correlated k distribution method for modeling nongray gaseous absorption, thermal emission, and multiple scattering in vertically inhomogeneous atmospheres. *J. Geophys. Res.*, **96**, 9027–9063.

Mischenko, M. I., and L. D. Travis, 1994: Light scattering by polydispersions of randomly oriented spheroids with sizes comparable to wavelengths of observation. *Appl. Opt.*, **33**, 7206–7225.

Mitchell, R. M., D. M. O'Brien, and B. W. Forgan, 1996: Calibration of the AVHRR shortwave channels: II. Application to NOAA 11 during early 1991. *Remote Sens. Environ.*, **55**, 139–152.

O'Brien, D. M., 1992: Accelerated quasi Monte Carlo integration of the radiative transfer equation. *J. Quant. Spectrosc. Radiat. Transfer*, **48**, 41–59.

O'Brien, D. M., 1998: Monte Carlo integration of the radiative transfer equation in a scattering medium with stochastic reflecting boundary. *J. Quant. Spectrosc. Radiat. Transfer*, **60**, 573–583.

O'Brien, D. M., and A. C. Dilley, 2000: Infrared cooling of the atmosphere: accuracy of correlated k-distributions. *J. Quant. Spectrosc. Radiat. Transfer*, **64**, 483–497.

O'Brien, D. M., R. M. Mitchell, and I. F. Grant, 1999: Observations of aerosol and BRDF at an Australian desert site. *Ocean color, land surface, radiation and clouds, aerosols: the contribution of POLDER and new generation spaceborne sensors to global change studies*, Méribel, France. Centre National D'Etudes Spatiales, 16 pp.

Stokes, G. G., 1852: On the composition and resolution of streams of polarized light from different sources. *Trans. Camb. Philos. Soc.*, **9**, 399.

van de Hulst, H. C., 1980: *Multiple light scattering. Tables, formulas, and applications. Volumes 1 and 2.* Academic Press, New York.

van de Hulst, H. C., 1981: *Light scattering by small particles.* Dover, New York.

τ	A	L	M	N	Iterations	I	Coulson
0.1	0	10	6	8	5	0.09079	0.08620
				16	5	0.08255	
				20	5	0.08582	
				24	5	0.08588	
				40	5	0.08600	
				64	5	0.08621	
0.1	0	1	6	64	5	0.08565	0.08620
		2			5	0.08617	
		5			5	0.08621	
		10			5	0.08621	

Table 1: Spot checks for the scattered intensity I seen by an observer looking towards the sun for a Rayleigh atmosphere with optical thickness $\tau = 0.1$ lying over a black surface with albedo $A = 0$. The solar zenith angle $\theta_\star$ is such that $\mu_\star = \cos\theta_\star = -0.4$. The number of layers is denoted by L, while M and N are the degrees of the azimuth and zenith quadratures.

τ	A	L	M	N	Iterations	I	Coulson
1.0	0.25	10	6	8	17	0.24171	0.25224
				16	17	0.25218	
				20	17	0.25215	
				24	17	0.25230	
				40	17	0.25245	
				64	17	0.25253	
1.0	0.25	1	6	64	15	0.27343	0.25224
		2			17	0.26165	
		5			17	0.25308	
		10			17	0.25253	
		20			17	0.25237	

Table 2: Spot checks for the scattered intensity I seen by an observer looking towards the sun for a Rayleigh atmosphere with optical thickness $\tau = 1$ lying over a Lambert surface with albedo $A = 0.25$. The solar zenith angle $\theta_\star$ is such that $\mu_\star = \cos\theta_\star = -0.4$. The number of layers is denoted by L, while M and N are the degrees of the azimuth and zenith quadratures.

τ	A	L	M	N	Iterations	I
0.2	0.25	10	6	20	9	1.3579
			12		8	1.2869
			16		8	1.2743
			20		8	1.2682
			24		8	1.2653
			36		8	1.2637
			48		8	1.2637
0.2	0.25	2	24	20	8	1.2707
		5			8	1.2660
		10			8	1.2653
		20			8	1.2651

Table 3: Spot checks for the scattered intensity I seen by an observer at the surface looking towards the sun for a composite atmosphere with molecular optical thickness $\tau_m = 0.1$, aerosol optical thickness $\tau_a = 0.1$ and scattering properties as described in the text. The surface is a Lambert reflector with albedo $A = 0.25$. The solar zenith angle $\theta_\star$ is such that $\mu_\star = \cos\theta_\star = -0.4$. The number of layers is denoted by L, while M and N are the degrees of the azimuth and zenith quadratures.

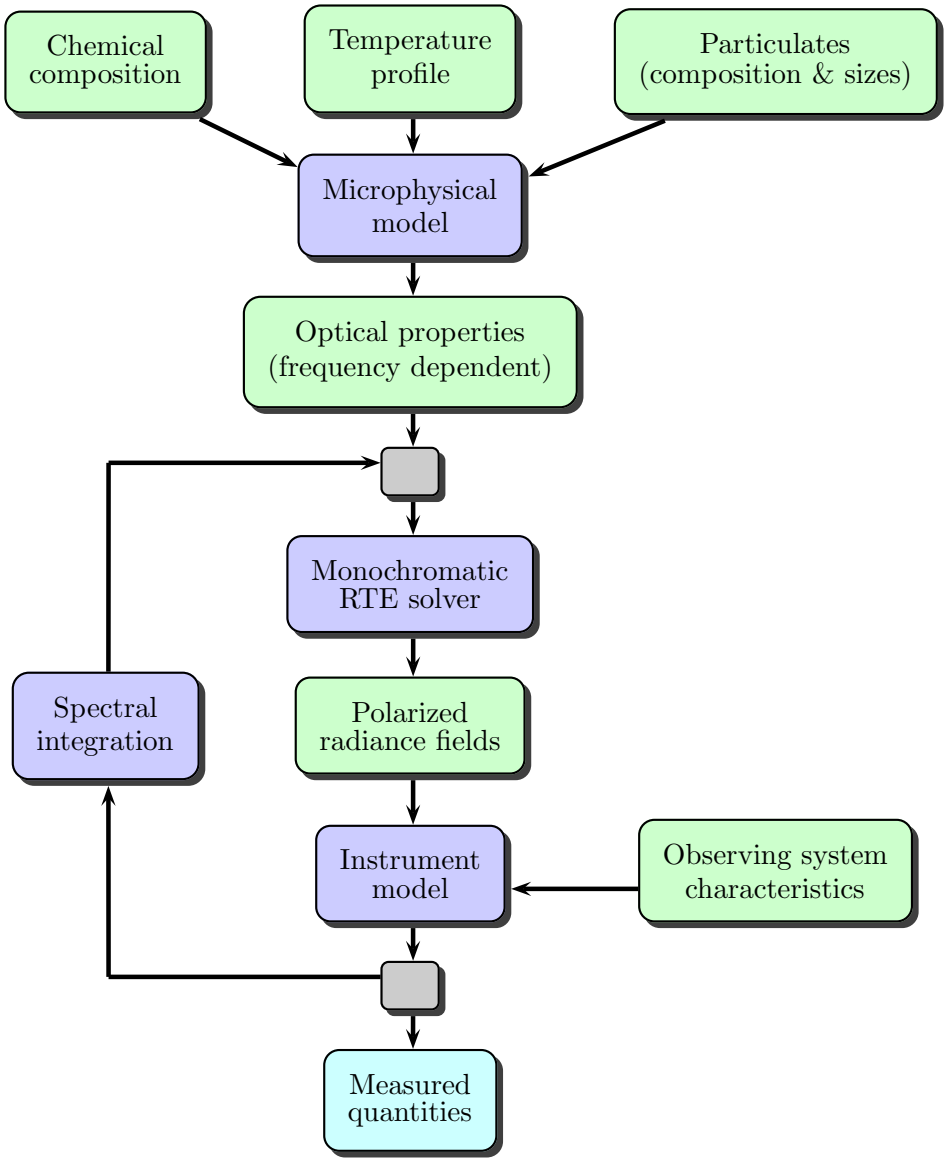

Figure 1: Flow chart of a radiation code. This report focuses on the monochromatic radiative transfer equation (RTE) solver and the instrument model for Cimel sun-photometers. The spectral integration, which will be covered in a separate report, uses correlated k-distributions to integrate over the rapidly varying spectral features within the band-passes of the instruments.

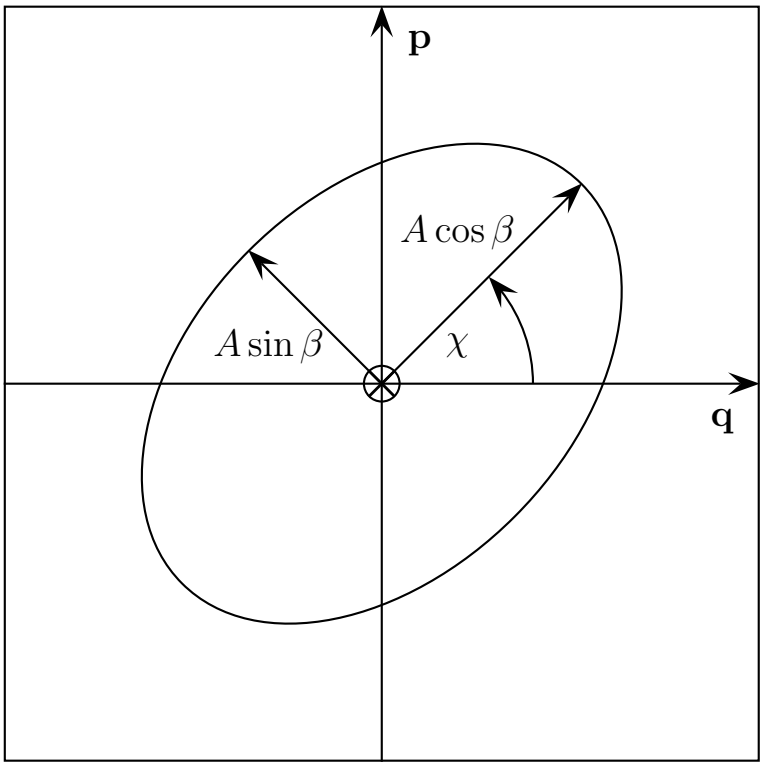

Figure 2: Polarization ellipse showing the coordinate frame. The propagation vector **r** is directed into the page. Vectors **q** and **r** define the reference plane for polarization of the beam, while vector **p** completes a right-handed orthonormal system.

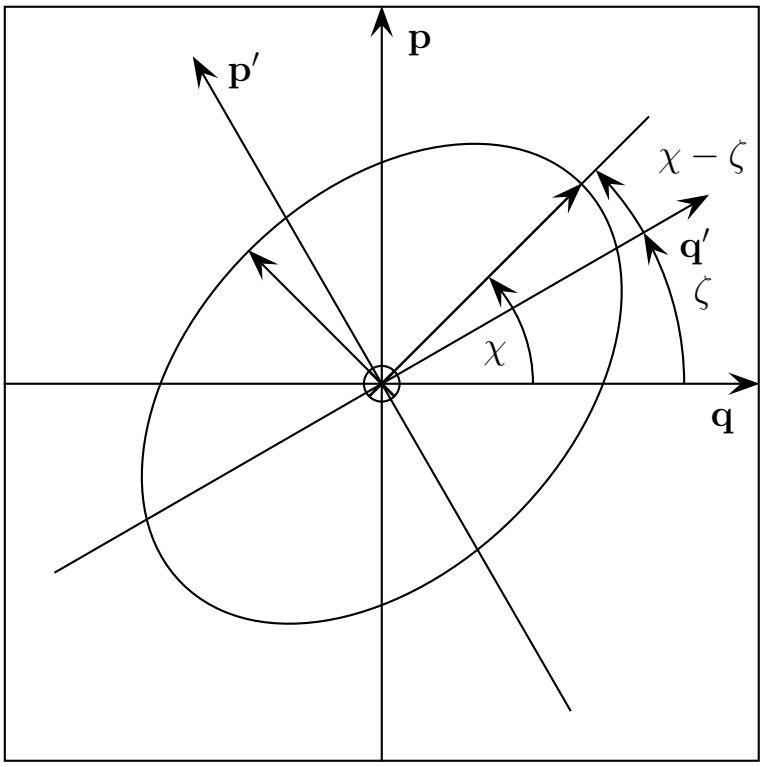

Figure 3: Vectors **p**, **q** and **r** (into the page) define a right-handed orthonormal coordinate system, with the reference plane for polarization determined by **q** and **r**. The primed vectors denote a coordinate system rotated about **r** through angle ζ. In the rotated frame, vectors $\mathbf{q}'$ and **r** define the reference plane for polarization.

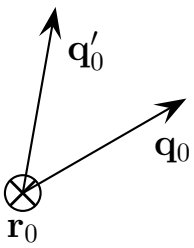

Figure 4: The vector $\mathbf{r}_0$ is directed into the page. Vectors $\mathbf{q}_0$ and $\mathbf{r}_0$ define the reference plane for polarization of the incident beam. Vectors $\mathbf{q}_0'$ and $\mathbf{r}_0$ lie in the plane of scattering.

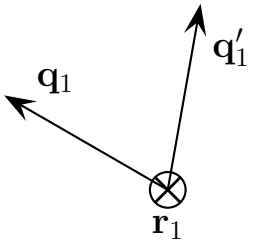

Figure 5: The vector $\mathbf{r}_1$ is directed into the page. Vectors $\mathbf{q}_1$ and $\mathbf{r}_1$ define the reference plane for polarization of the scattered beam. Vectors $\mathbf{q}_1'$ and $\mathbf{r}_1$ lie in the plane of scattering.

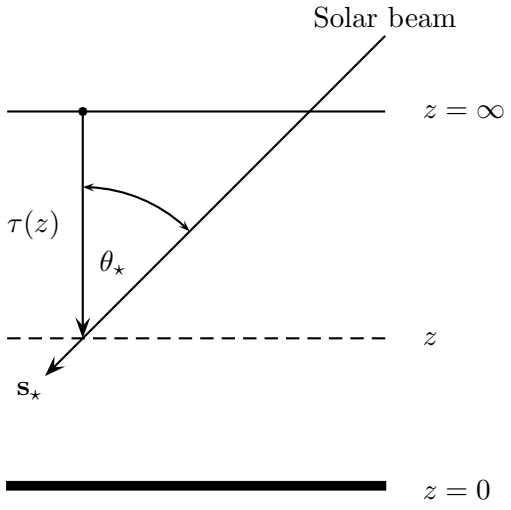

Figure 6: Geometry of the solar beam.

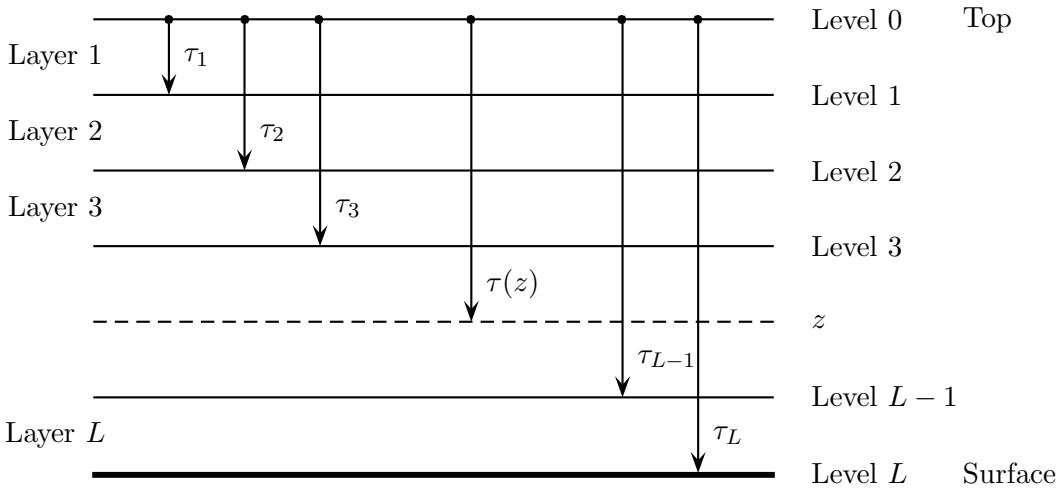

Figure 7: Labelling conventions for the layered atmosphere.

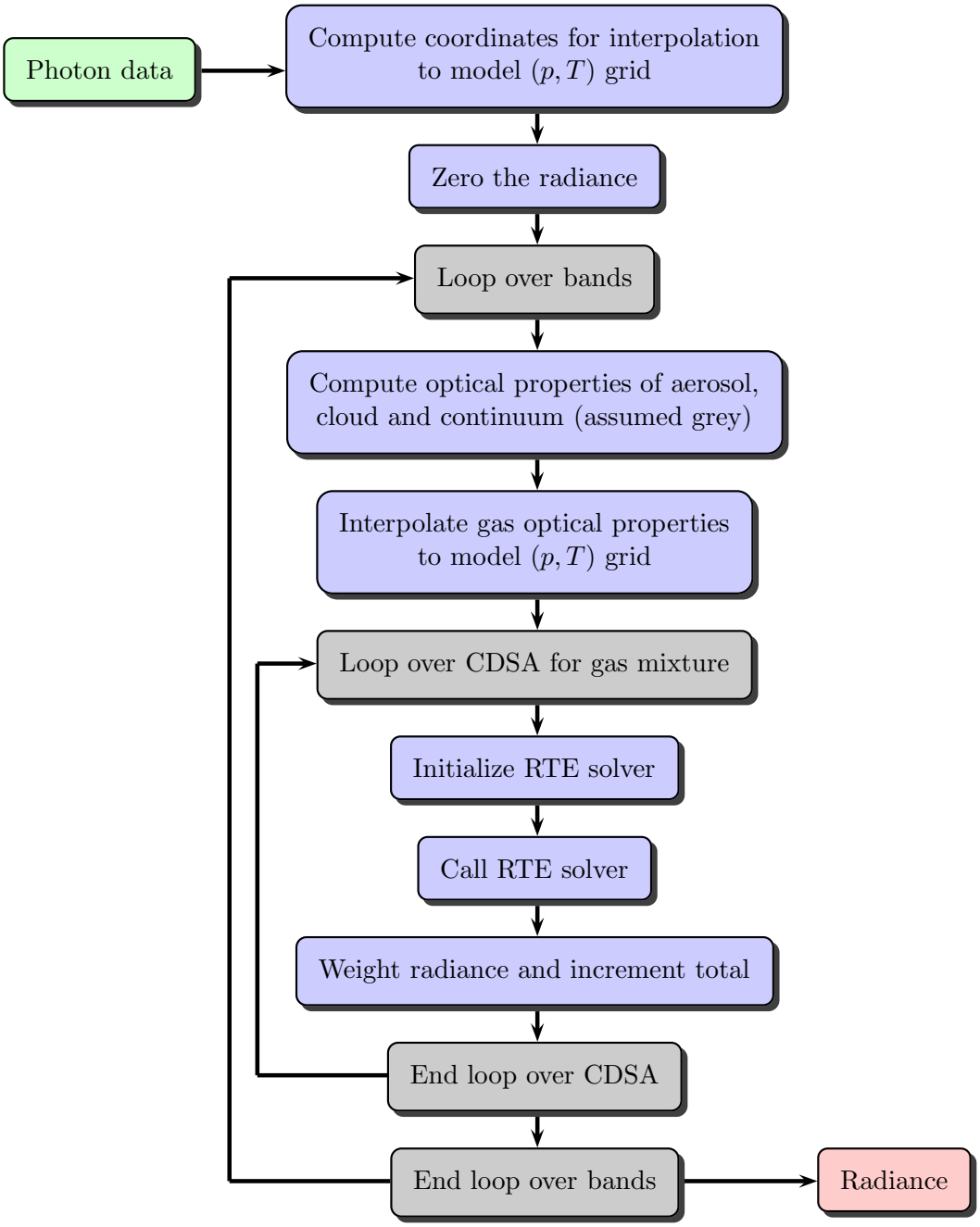

Figure 8: Flow chart for subroutine Radiation. Note that CDSA stands for correlated distribution of specific absorption.

```
!!!!
!
!     TYPE Radiance_Data
!     ******************
!
!!!!
      TYPE    ::  Radiance_Data
          INTEGER                                  ::  NumLayers
          INTEGER                                  ::  NumComponents
          INTEGER                                  ::  NumIterations
          INTEGER                                  ::  MaxIterations
          TYPE (Stokes_Vector),   POINTER,&
                                  DIMENSION(:)     ::  RDir
          TYPE (Stokes_Vector),   POINTER,&
                                  DIMENSION(:)     ::  RSca
          TYPE (Stokes_Vector),   POINTER,&
                                  DIMENSION(:)     ::  RTot
          REAL (LongReal),        POINTER,&
                                  DIMENSION(:)     ::  FDirUp
          REAL (LongReal),        POINTER,&
                                  DIMENSION(:)     ::  FScaUp
          REAL (LongReal),        POINTER,&
                                  DIMENSION(:)     ::  FTotUp
          REAL (LongReal),        POINTER,&
                                  DIMENSION(:)     ::  FDirDown
          REAL (LongReal),        POINTER,&
                                  DIMENSION(:)     ::  FScaDown
          REAL (LongReal),        POINTER,&
                                  DIMENSION(:)     ::  FTotDown
          TYPE (Profile_Table),   POINTER,&
                                  DIMENSION(:)     ::  Polarization
          TYPE (Profile_Table),   POINTER,&
                                  DIMENSION(:)     ::  RubensonPolarization
      END TYPE Radiance_Data
```

Figure 9: Code defining the components of type Radiance_Data.

```
!!!!
!
!     TYPE Stokes_Vector
!     ******************
!
!!!!
      TYPE    ::  Stokes_Vector
          TYPE (Stokes_Vector_Table), POINTER,&
                                      DIMENSION(:)    ::  Vector
      END TYPE Stokes_Vector
```

Figure 10: Code defining the components of type Stokes_Vector.

```
!!!!
!
!     TYPE Stokes_Vector_Table
!     ************************
!
!!!!
      TYPE    ::  Stokes_Vector_Table
          REAL (LongReal),    POINTER,&
                              DIMENSION(:,:)  ::  Table
      END TYPE Stokes_Vector_Table
```

Figure 11: Code defining the components of type Stokes_Vector_Table.

```
!!!!
!
!     TYPE Phase_Matrix
!     *****************
!
!!!!
      TYPE    ::  Phase_Matrix
          TYPE (Phase_Matrix_Table),  POINTER,&
                                      DIMENSION(:,:)  ::  Matrix
      END TYPE Phase_Matrix
```

Figure 12: Code defining the components of type Phase_Matrix.

```
!!!!
!
!     TYPE Phase_Matrix_Table
!     ***********************
!
!!!!
      TYPE    ::  Phase_Matrix_Table
          REAL (LongReal),    POINTER,&
                              DIMENSION(:,:,:)    ::  Table
          REAL (LongReal),    POINTER,&
                              DIMENSION(:,:)      ::  TableSun
      END TYPE Phase_Matrix_Table
```

Figure 13: Code defining the components of type Phase_Matrix_Table.

```
!!!!
!
!     TYPE Optics_Data
!     ****************
!
!     AbsOT           :   a pointer to an array with dimension NumLayers
!                         containing the absorption optical thickness,
!                         layer by layer.
!     ScaOT           :   a pointer to an array with dimension NumLayers
!                         containing the scattering optical thickness,
!                         layer by layer.
!     ExtOT           :   a pointer to an array with dimension NumLayers
!                         containing the extinction optical thickness,
!                         layer by layer.
!     Albedo          :   a pointer to an array with dimension NumLayers
!                         containing the single scattering albedo,
!                         layer by layer.
!     Asymmetry       :   a pointer to an array with dimension NumLayers
!                         containing the asymmetry parameter of the
!                         scattering phase function, layer by layer.
!
!!!!
      TYPE    ::  Optics_Data
          INTEGER                                   ::  NumLayers
          INTEGER                                   ::  NumLayersPhase
          CHARACTER (LenType)                       ::  Type
          REAL (LongReal),        POINTER,&
                                  DIMENSION(:)      ::  AbsOT
          REAL (LongReal),        POINTER,&
                                  DIMENSION(:)      ::  ScaOT
          REAL (LongReal),        POINTER,&
                                  DIMENSION(:)      ::  ExtOT
          REAL (LongReal),        POINTER,&
                                  DIMENSION(:)      ::  Albedo
          REAL (LongReal),        POINTER,&
                                  DIMENSION(:)      ::  Asymmetry
          TYPE (Phase_Matrix),    POINTER,&
                                  DIMENSION(:)      ::  Phase
      END TYPE Optics_Data
```

Figure 14: Code defining the components of type Optics_Data.

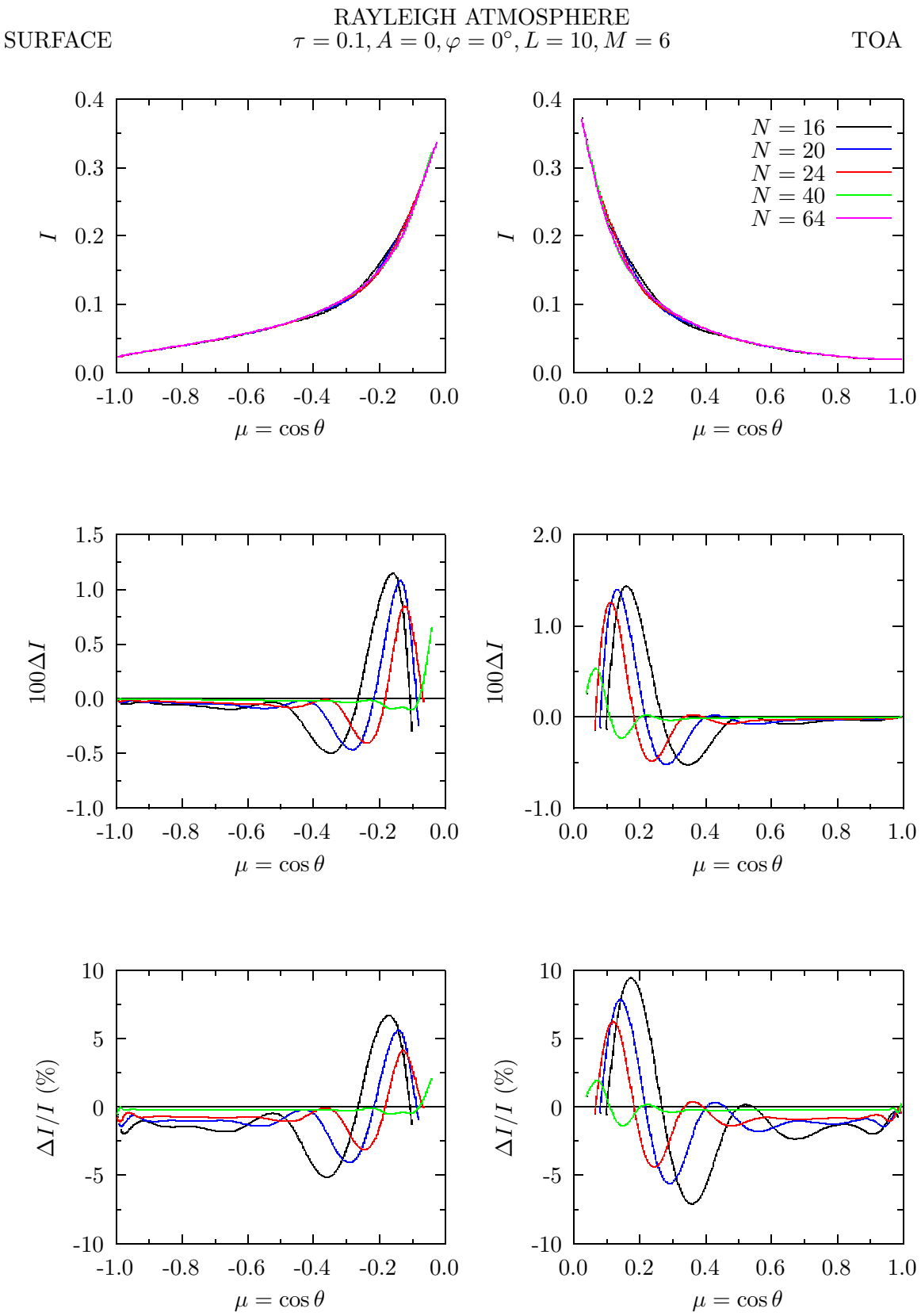

Figure 15: The three rows show the value, absolute error (×100) and relative error in the intensity I of the scattered radiance obtained with different orders of gaussian quadrature for the zenith integration. The columns refer to surface and TOA values.

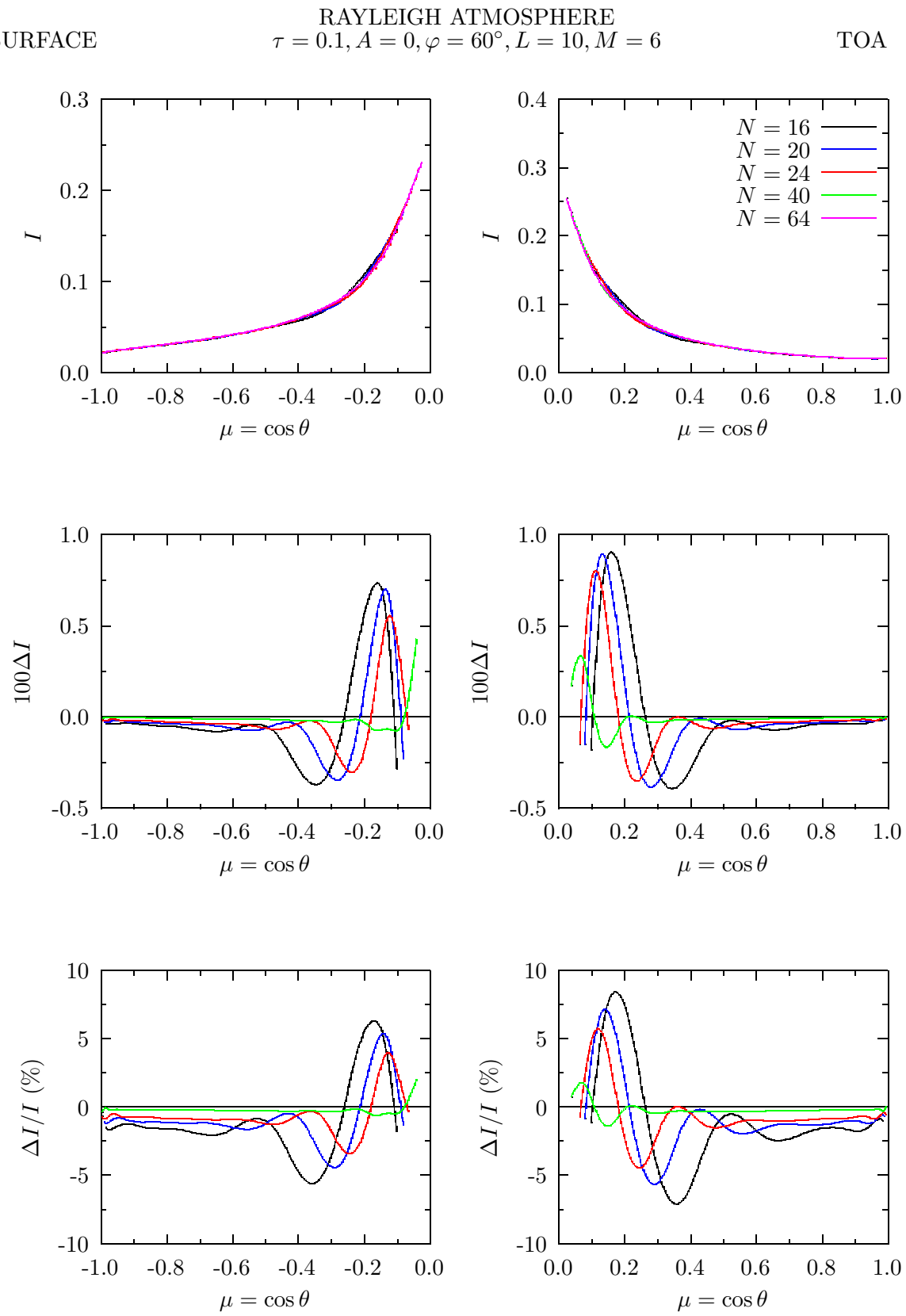

Figure 16: The three rows show the value, absolute error (×100) and relative error in the intensity I of the scattered radiance obtained with different orders of gaussian quadrature for the zenith integration. The columns refer to surface and TOA values.

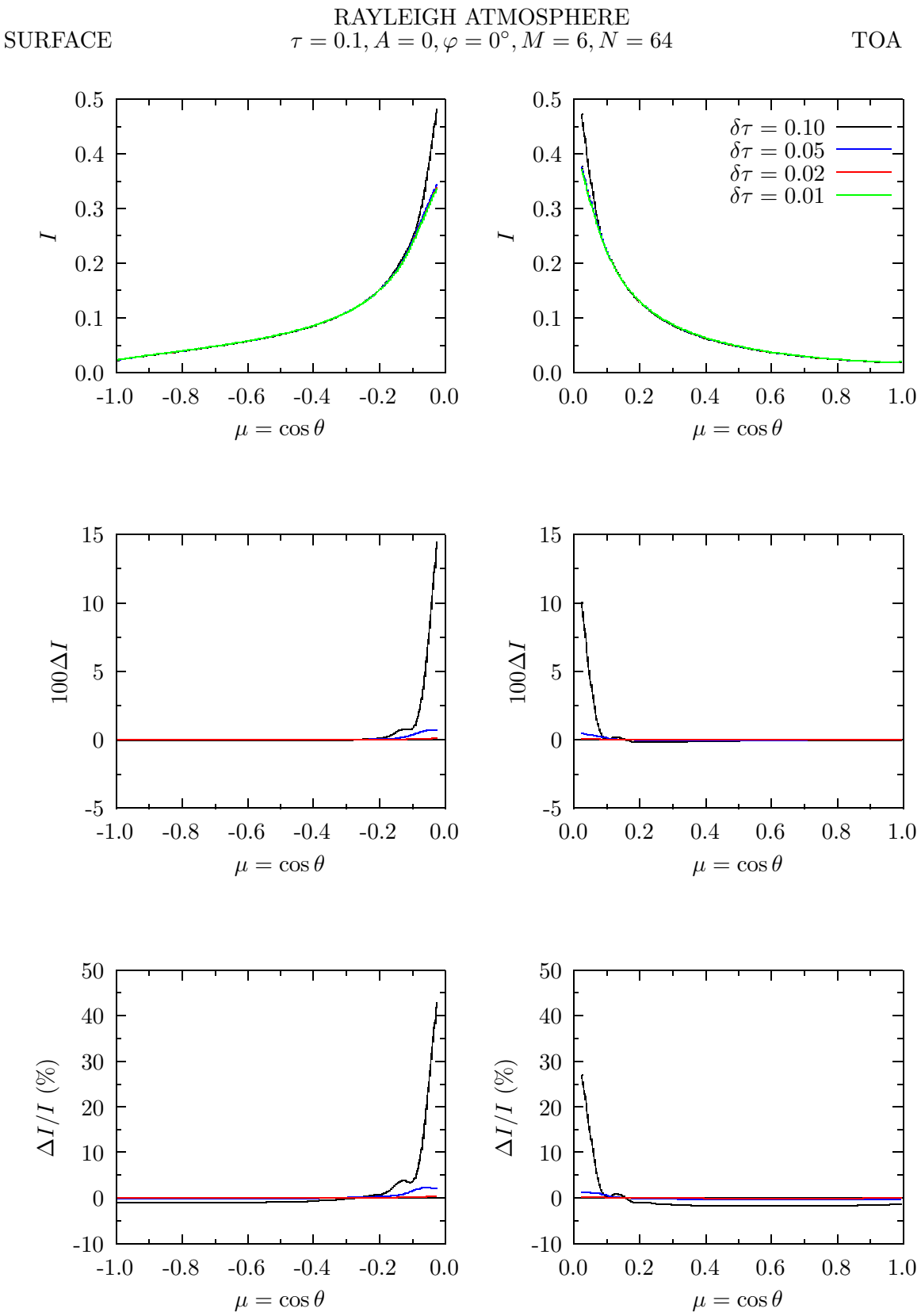

Figure 17: The three rows show the value, absolute error (×100) and relative error in the intensity I of the scattered radiance obtained with different numbers of levels in the optical depth integration. The columns refer to surface and TOA values.

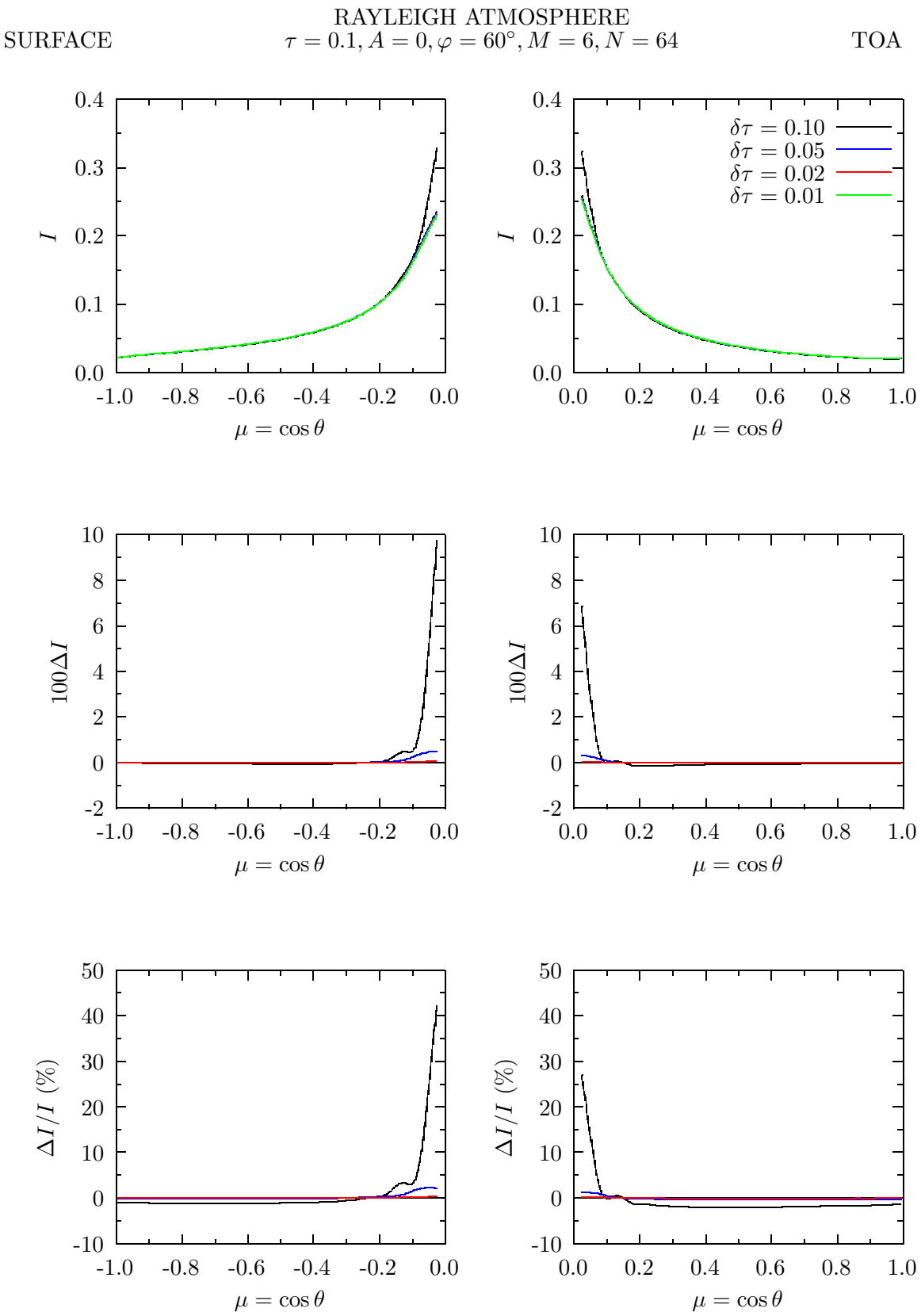

Figure 18: The three rows show the value, absolute error (×100) and relative error in the intensity I of the scattered radiance obtained with different numbers of levels in the optical depth integration. The columns refer to surface and TOA values.

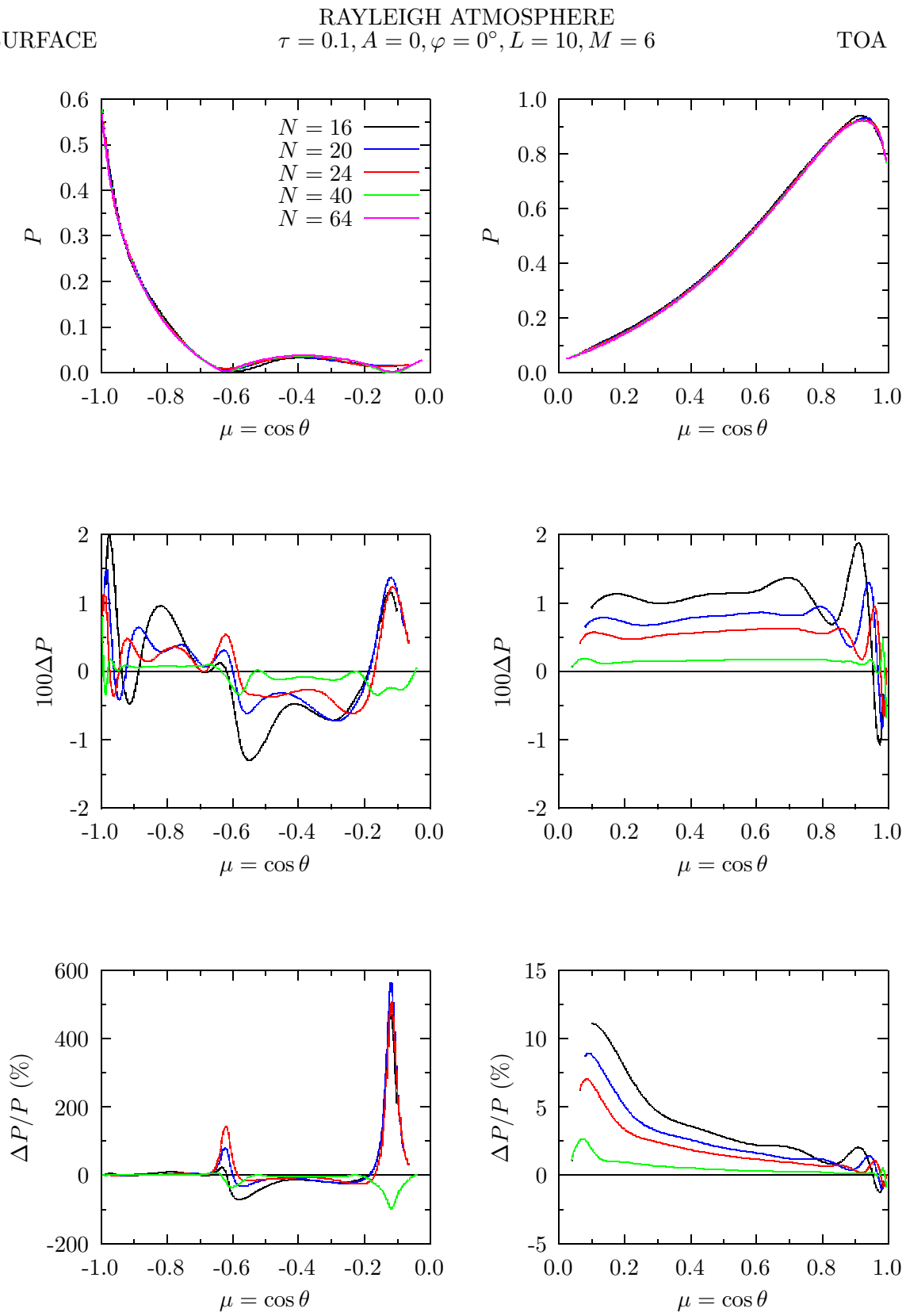

Figure 19: The three rows show the value, absolute error (×100) and relative error in the polarization P obtained with different orders of gaussian quadrature for the zenith integration. The columns refer to surface and TOA values.

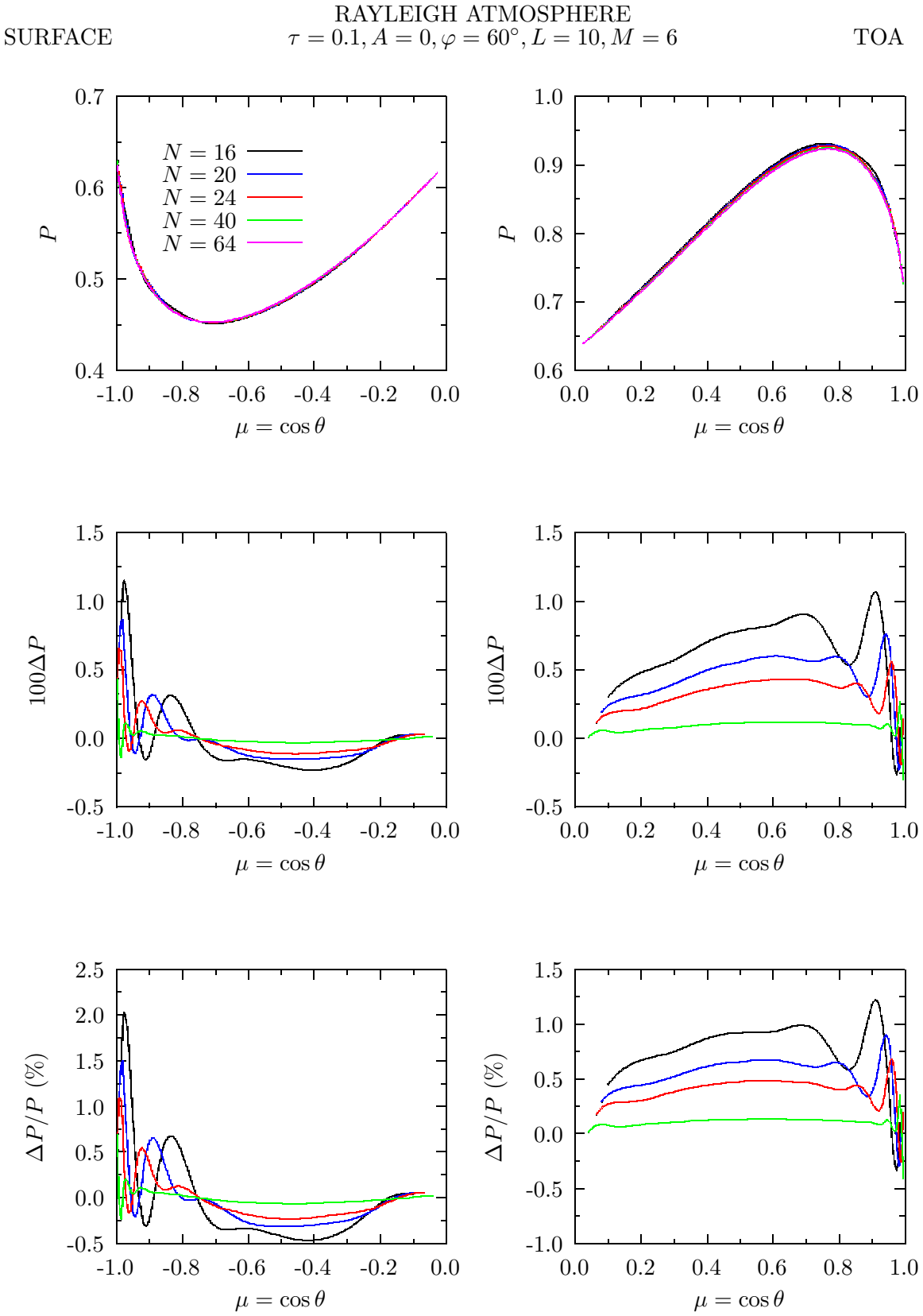

Figure 20: The three rows show the value, absolute error (×100) and relative error in the polarization P obtained with different orders of gaussian quadrature for the zenith integration. The columns refer to surface and TOA values.

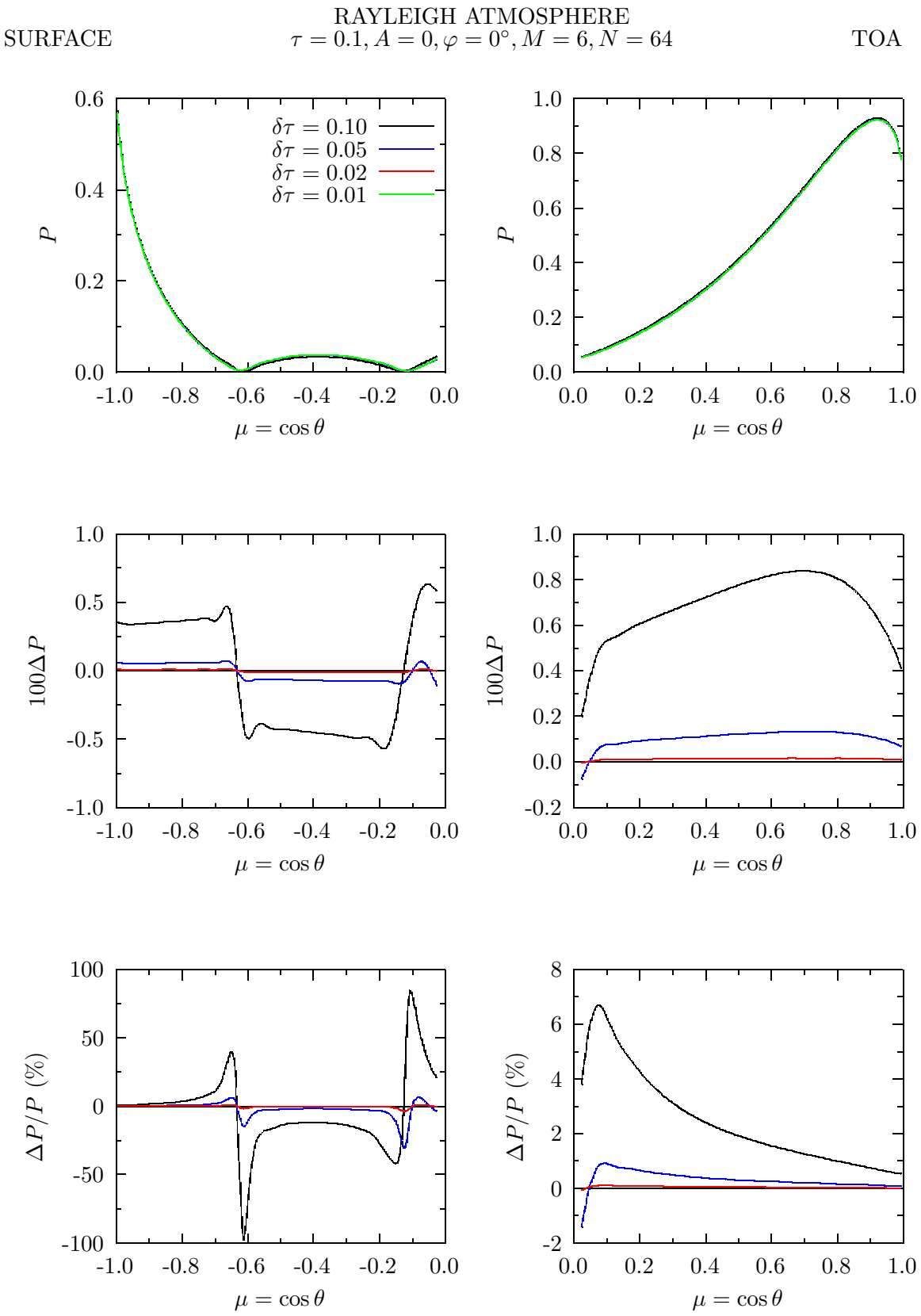

Figure 21: The three rows show the value, absolute error (×100) and relative error in the polarization P obtained with different numbers of levels in the optical depth integration. The columns refer to surface and TOA values.

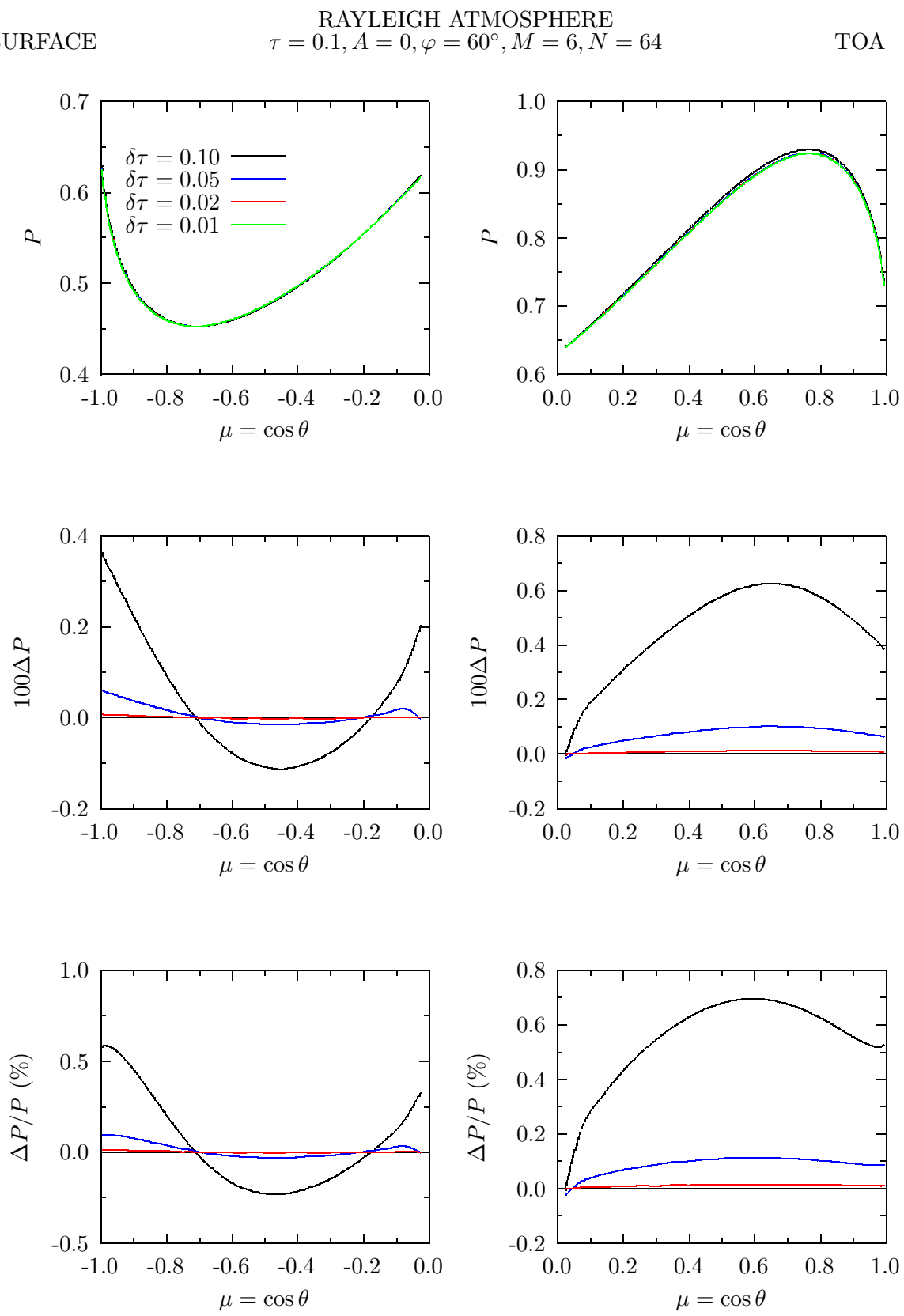

Figure 22: The three rows show the value, absolute error (×100) and relative error in the polarization P obtained with different numbers of levels in the optical depth integration. The columns refer to surface and TOA values.

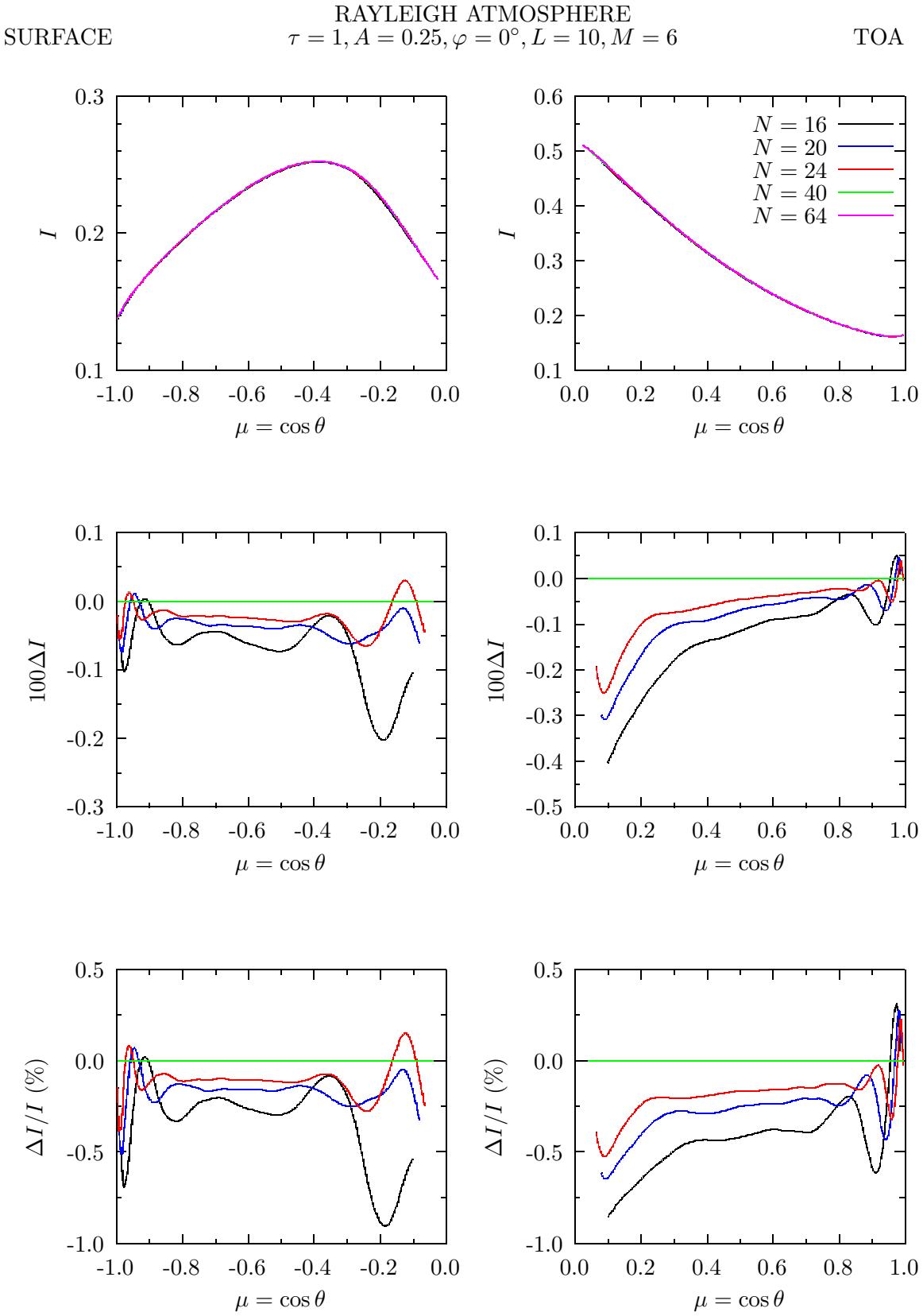

Figure 23: The three rows show the value, absolute error (×100) and relative error in the intensity I of the scattered radiance obtained with different orders of gaussian quadrature for the zenith integration. The columns refer to surface and TOA values.

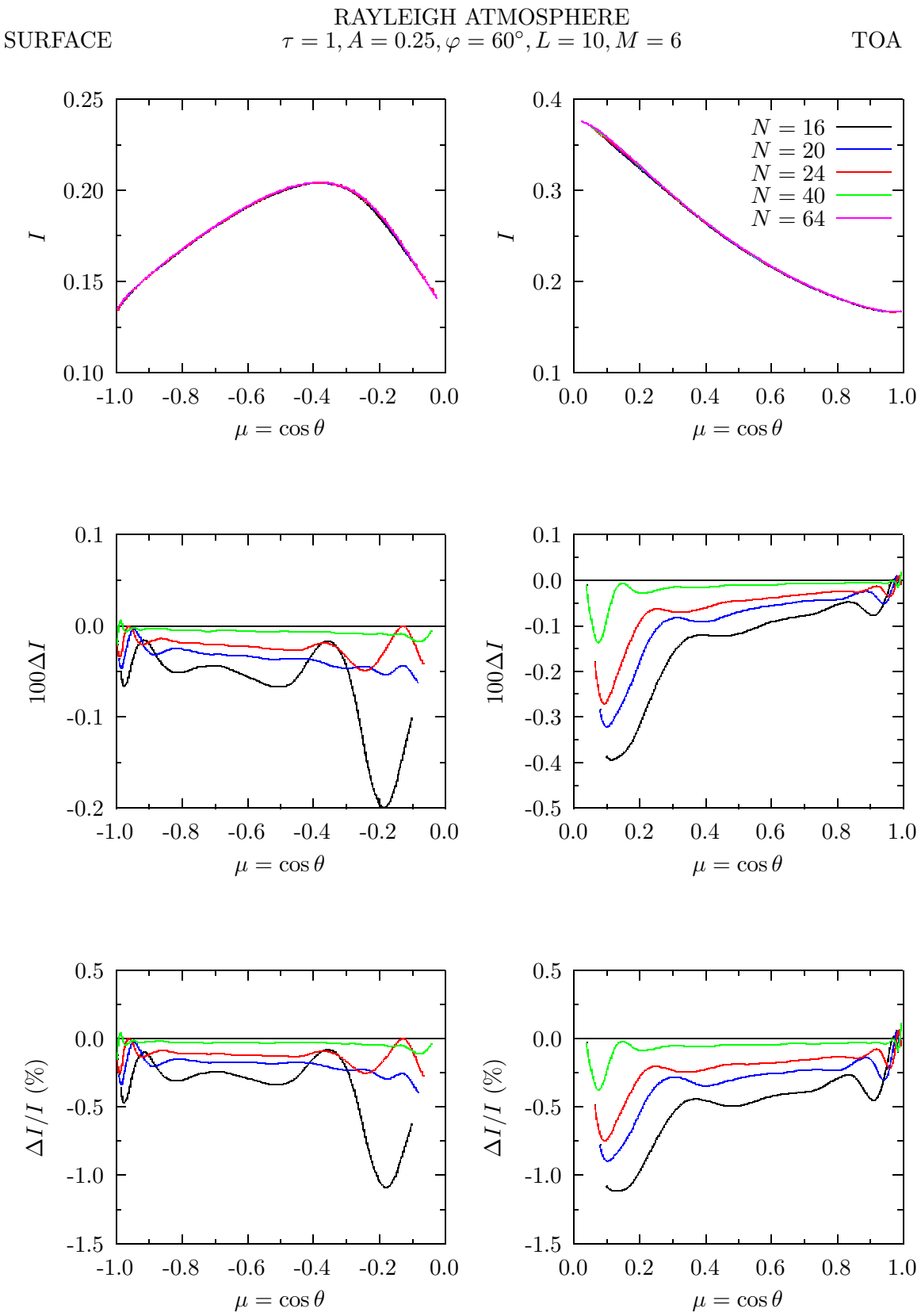

Figure 24: The three rows show the value, absolute error (×100) and relative error in the intensity I of the scattered radiance obtained with different orders of gaussian quadrature for the zenith integration. The columns refer to surface and TOA values.

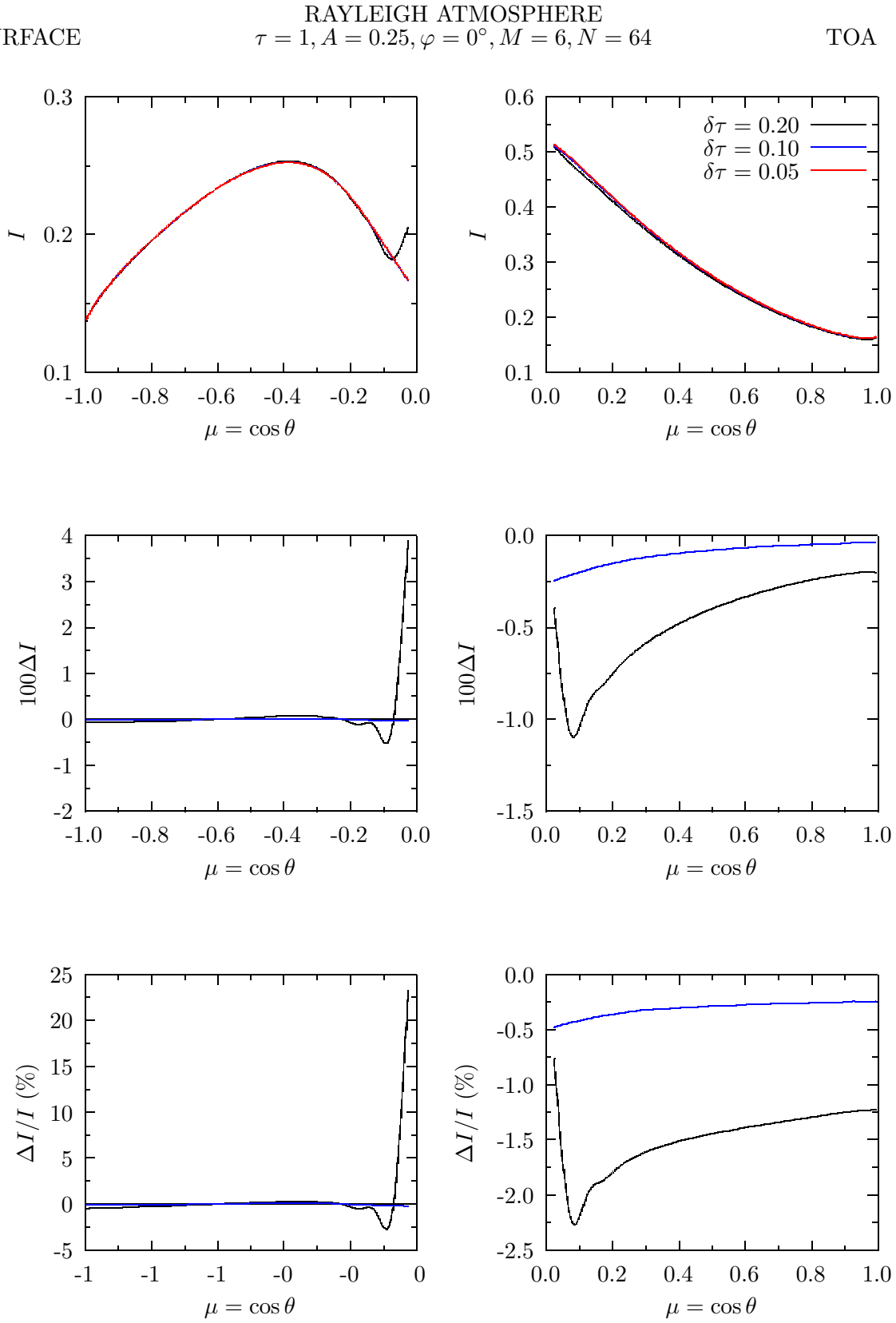

Figure 25: The three rows show the value, absolute error (×100) and relative error in the intensity I of the scattered radiance obtained with different numbers of levels in the optical depth integration. The columns refer to surface and TOA values.

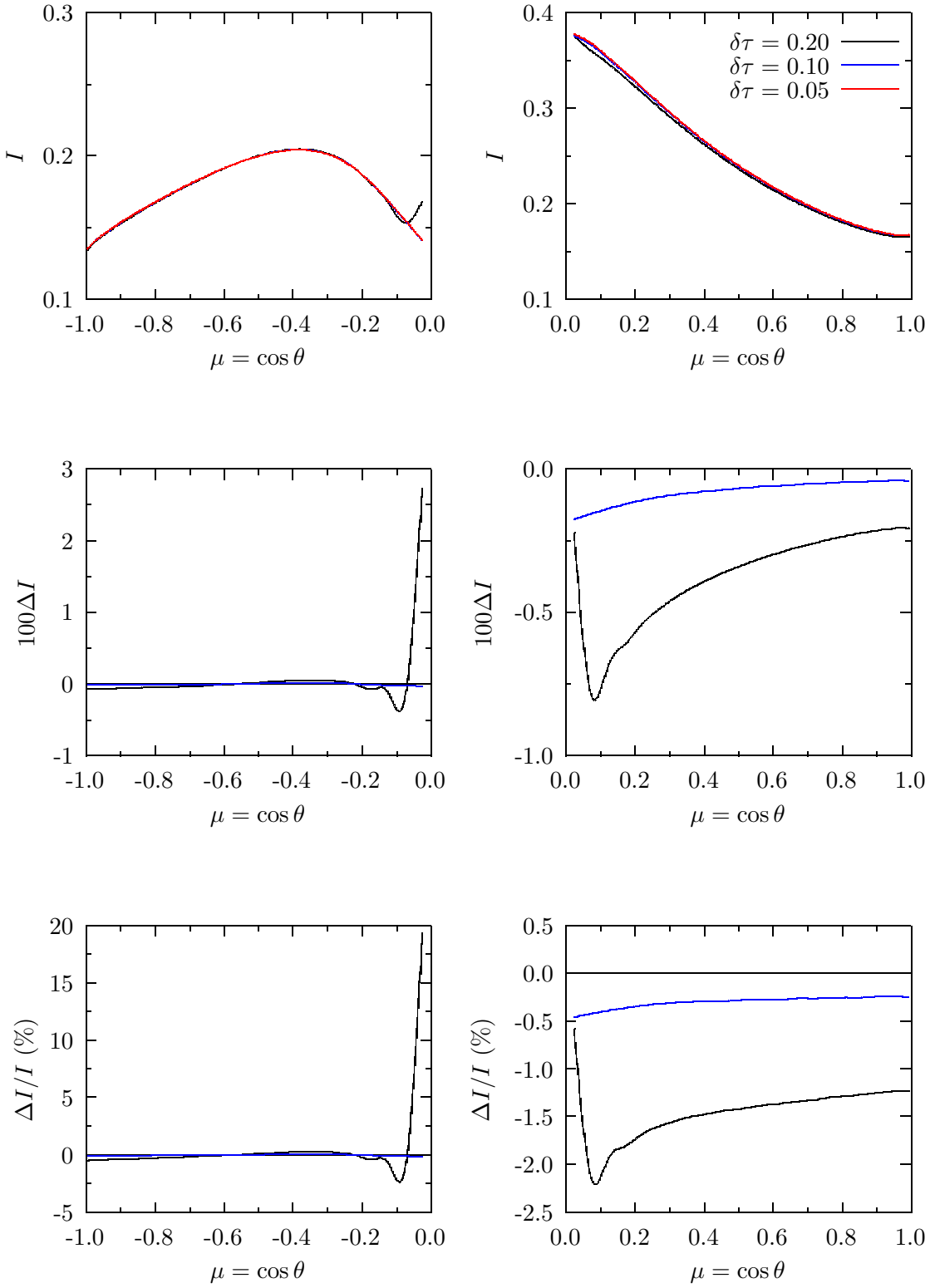

Figure 26: The three rows show the value, absolute error (×100) and relative error in the intensity I of the scattered radiance obtained with different numbers of levels in the optical depth integration. The columns refer to surface and TOA values.

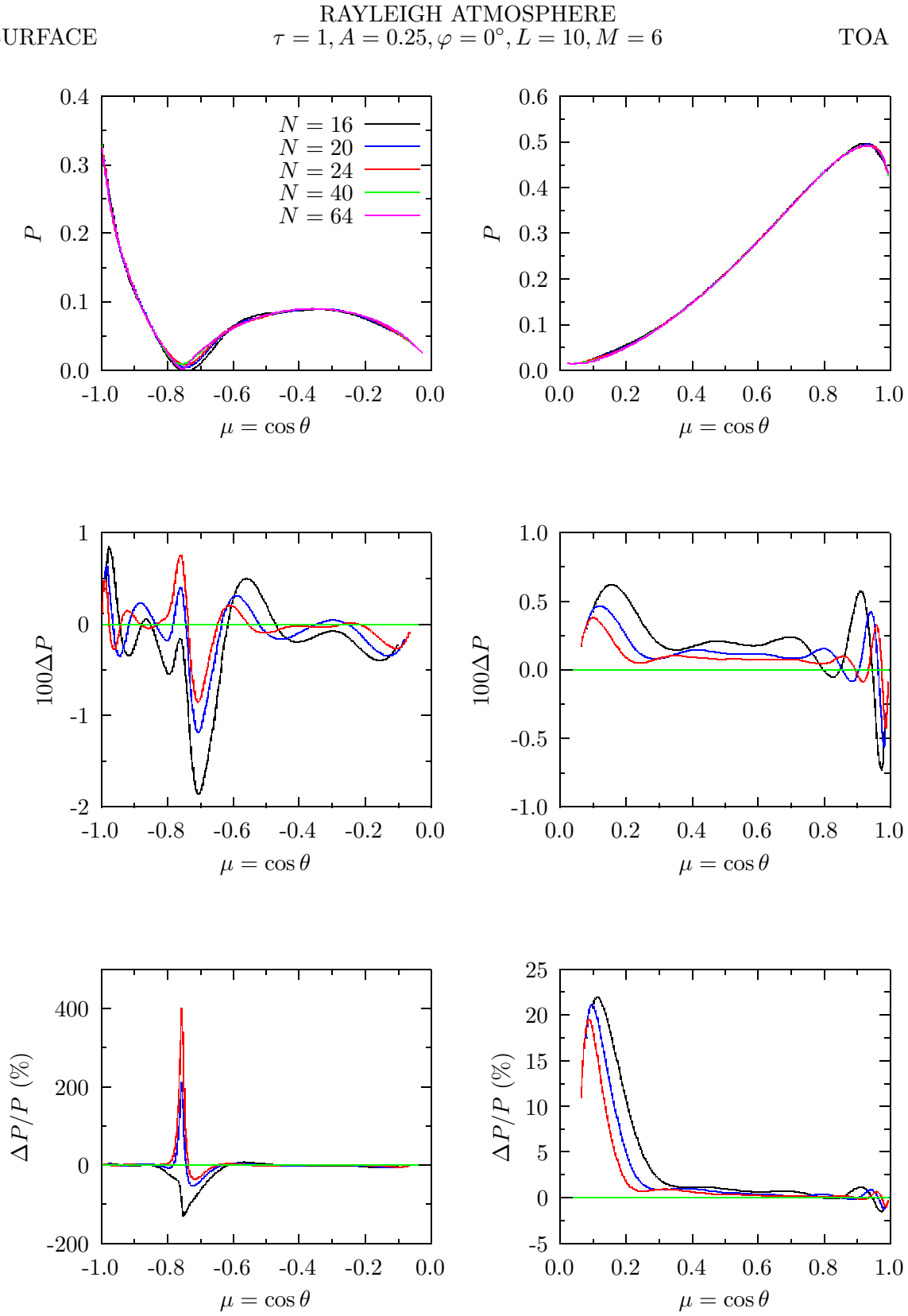

Figure 27: The three rows show the value, absolute error (×100) and relative error in the polarization P obtained with different orders of gaussian quadrature for the zenith integration. The columns refer to surface and TOA values.

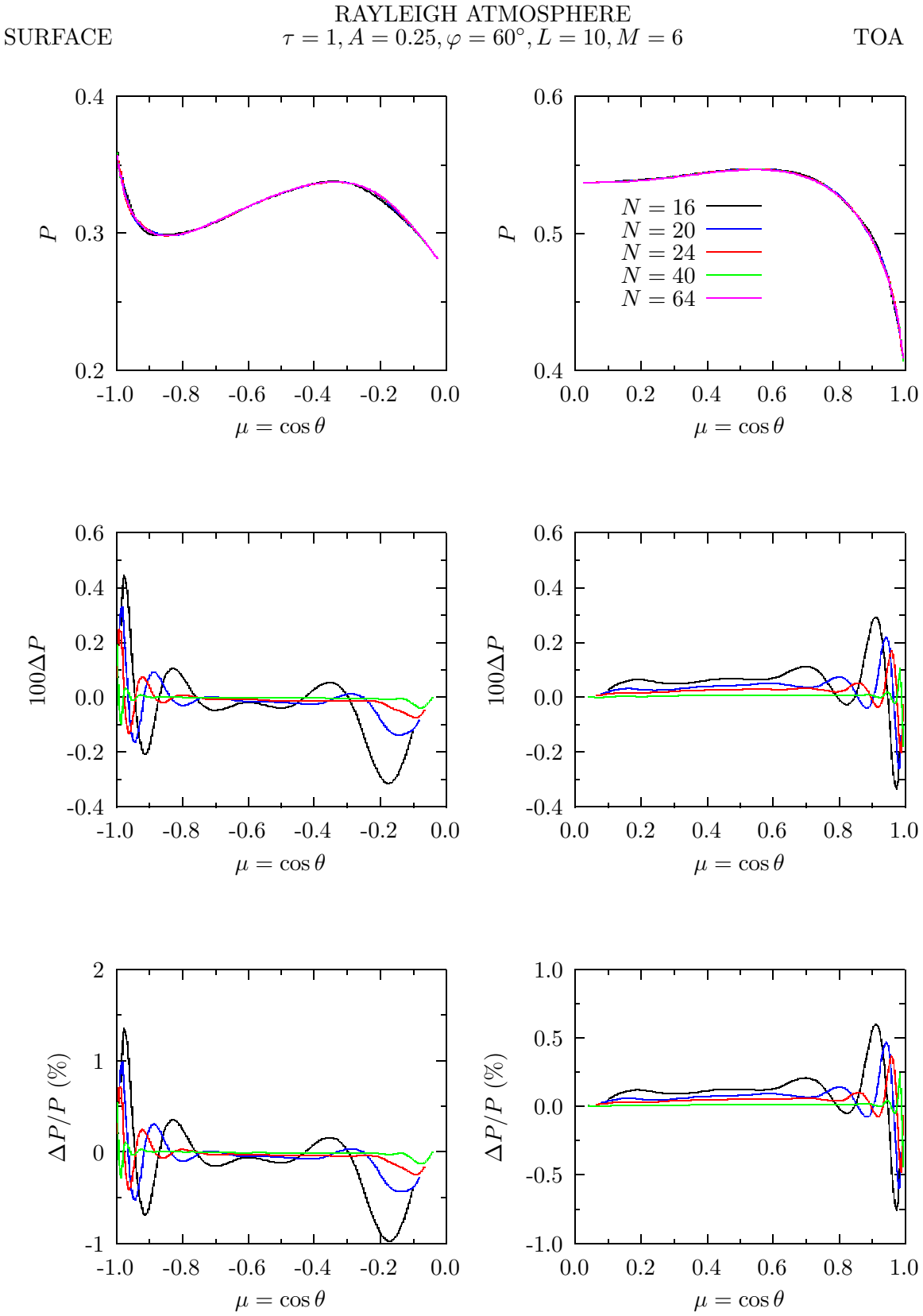

Figure 28: The three rows show the value, absolute error (×100) and relative error in the polarization P obtained with different orders of gaussian quadrature for the zenith integration. The columns refer to surface and TOA values.

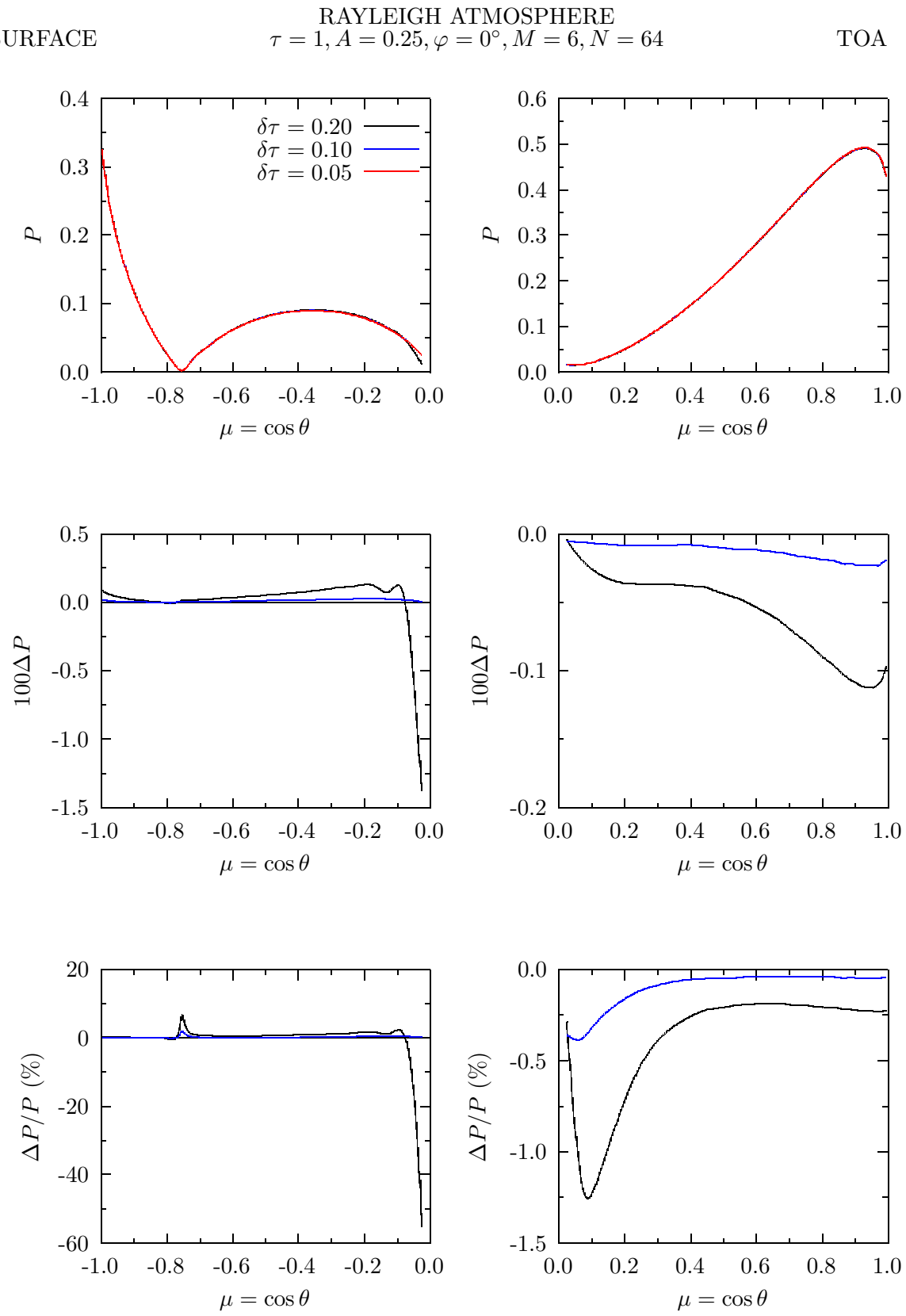

Figure 29: The three rows show the value, absolute error (×100) and relative error in the polarization P obtained with different numbers of levels in the optical depth integration. The columns refer to surface and TOA values.

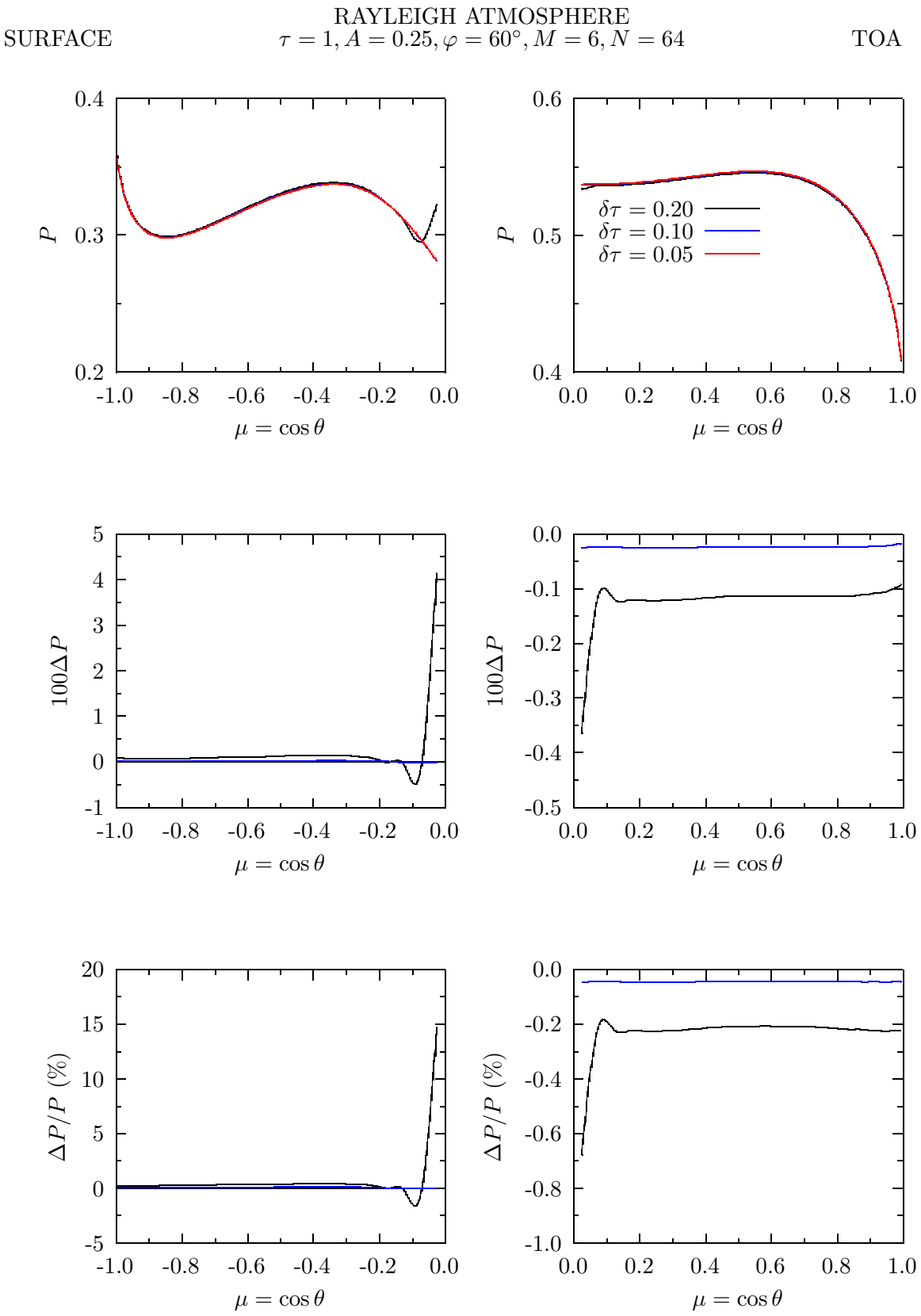

Figure 30: The three rows show the value, absolute error (×100) and relative error in the polarization P obtained with different numbers of levels in the optical depth integration. The columns refer to surface and TOA values.

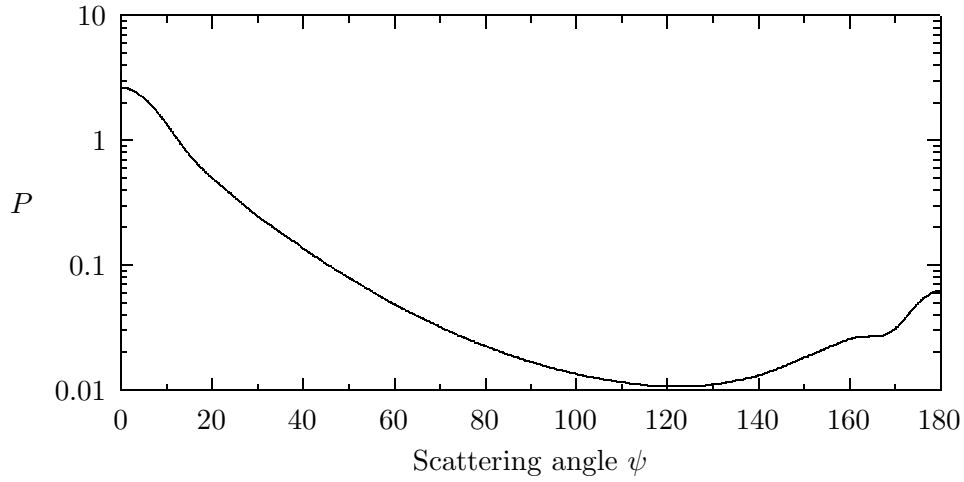

Figure 31: Unpolarized scattering phase function for the aerosol particles used in the test case with both molecular and aerosol scattering. (Note that the full polarized scattering matrix was used in the calculations.)

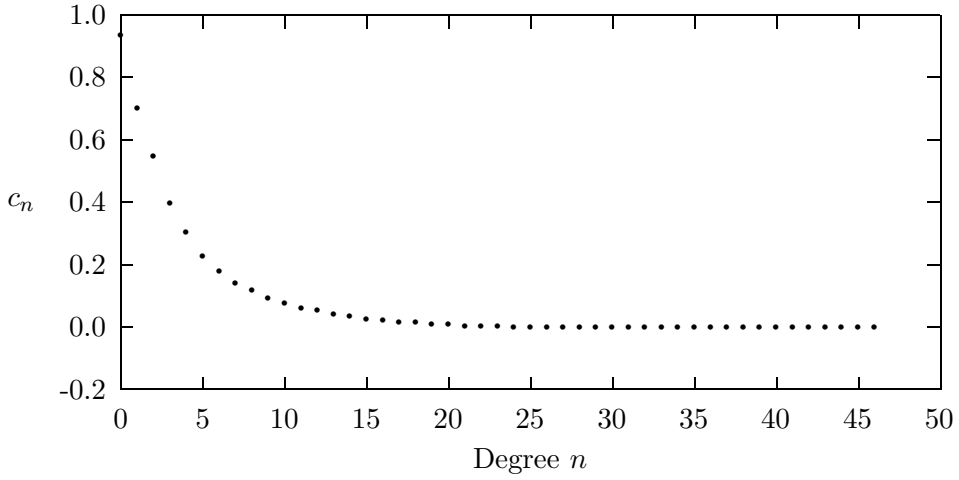

Figure 32: Coefficients of the expansion of the scattering function M_1 in Legendre series, $M_1(\cos\psi) = \sum_{n=0}^{\infty}(2n+1)c_n P_n(\cos\psi)$.

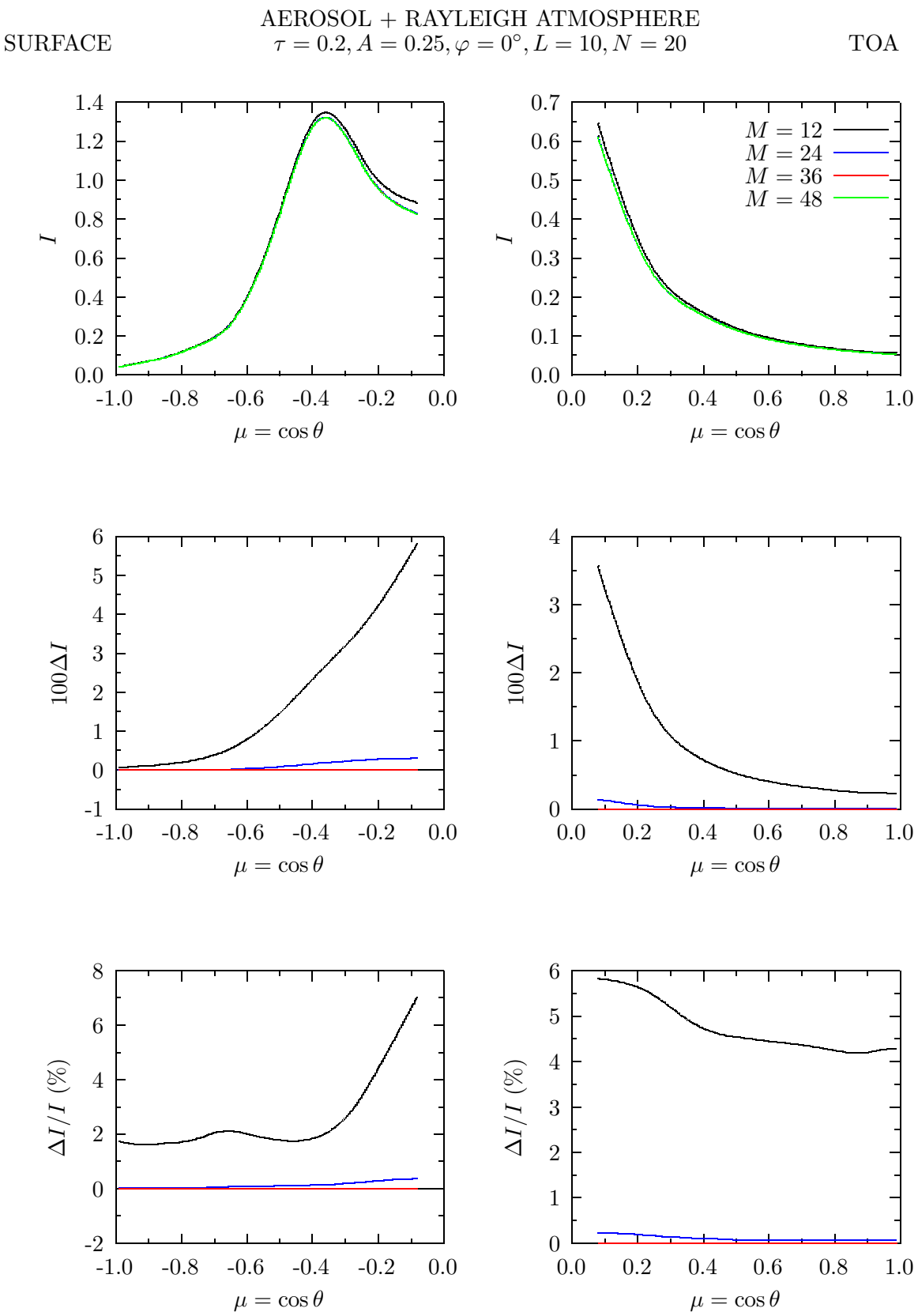

Figure 33: The three rows show the value, absolute error (×100) and relative error in the intensity I of the scattered radiance obtained with different orders of trapezoidal quadrature in the azimuth integration. The columns refer to surface and TOA values.

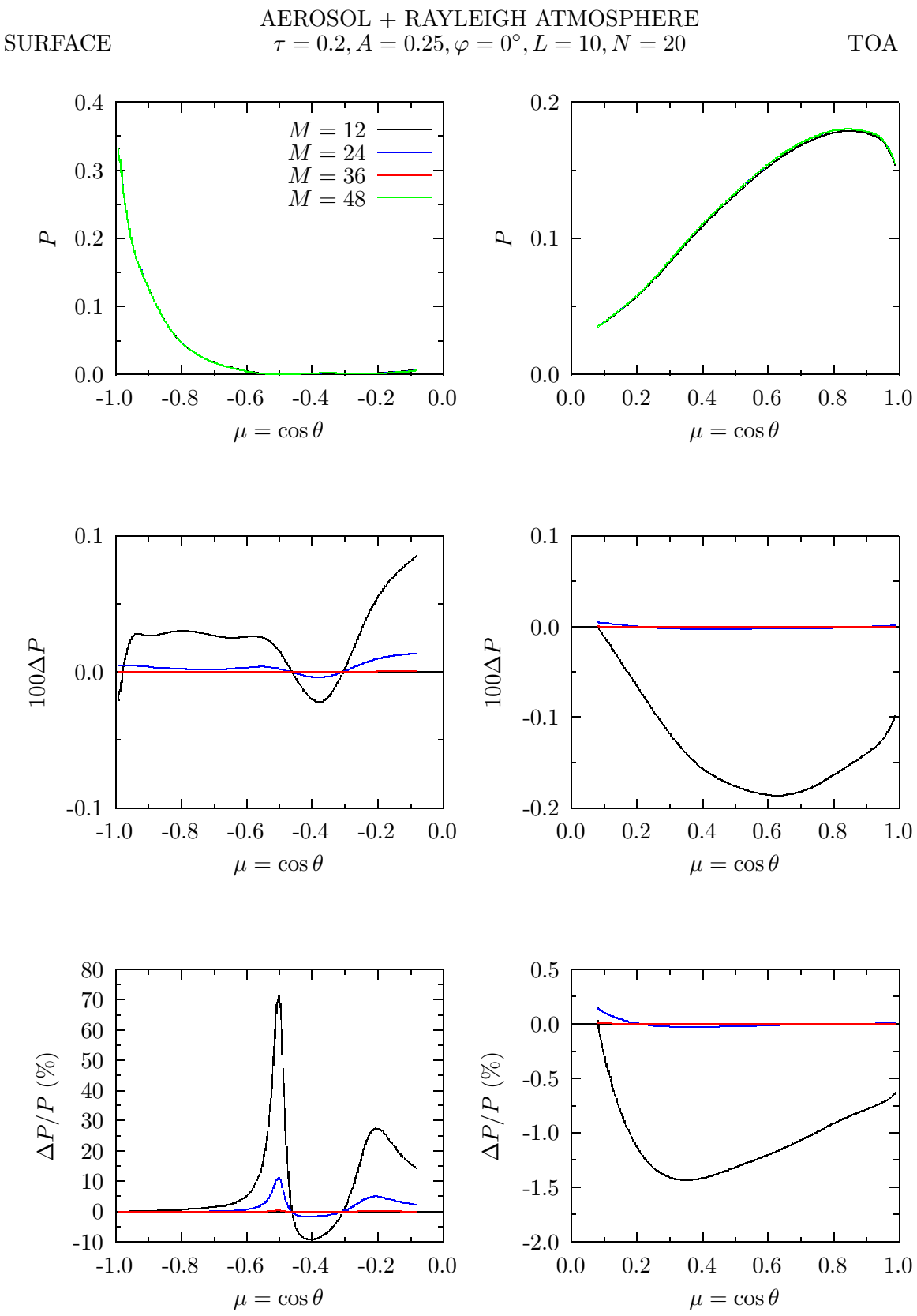

Figure 34: The three rows show the value, absolute error (×100) and relative error in the polarization P obtained with different orders of trapezoidal quadrature in the azimuth integration. The columns refer to surface and TOA values.

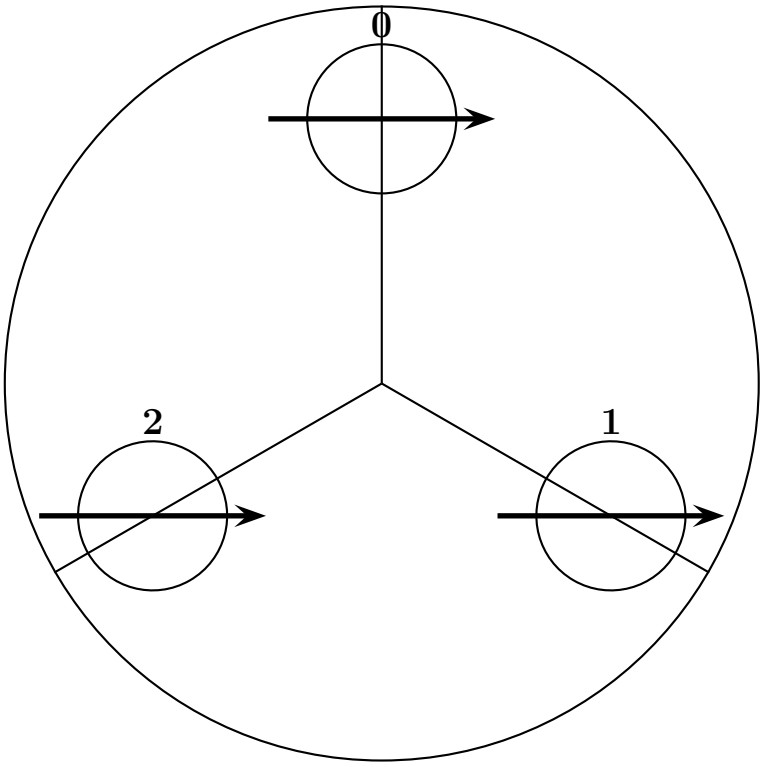

Figure 35: Cimel sun-photometer filter wheel showing the positions of the filters for the polarized channels. The wheel is covered by a sheet of polarizing material with the axis for maximum transmission indicated by the arrows. The instrument samples the filter located at the top of the diagram. Thus, when the filters are rotated into position, the angle of polarization changes by 120° between successive filters.

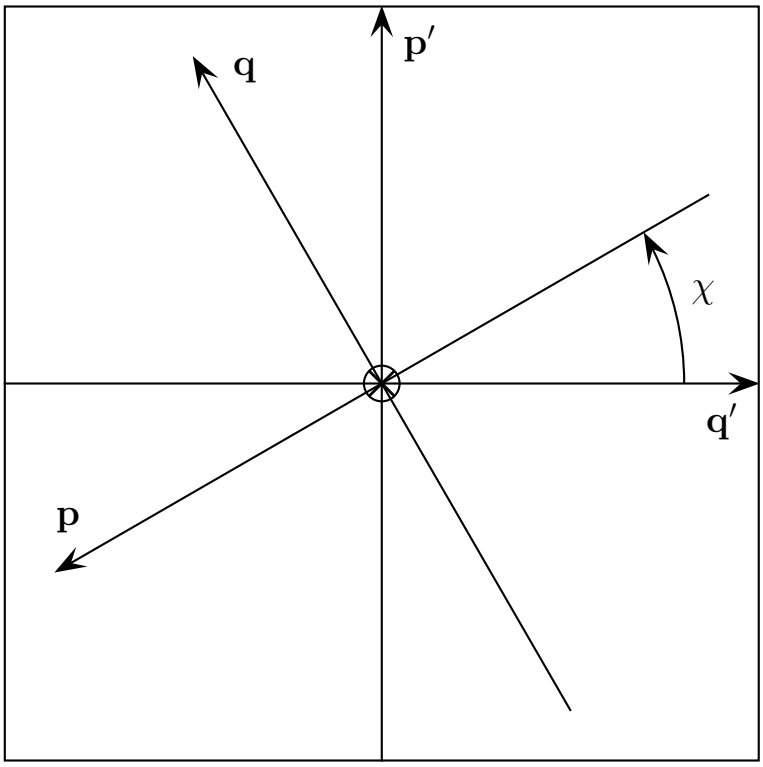

Figure 36: Vectors $\mathbf{p}'$, $\mathbf{q}'$ and $\mathbf{r}'$ (into the page) define a right-handed orthonormal coordinate system, with the reference plane for polarization of the incident radiance determined by $\mathbf{q}'$ and $\mathbf{r}'$. The unprimed vectors denote a coordinate system, rotated about $\mathbf{r}'$ through angle χ, with vectors $\mathbf{q}$ and $\mathbf{r}$ defining the plane of maximum transmittance for a linear polarizing filter.

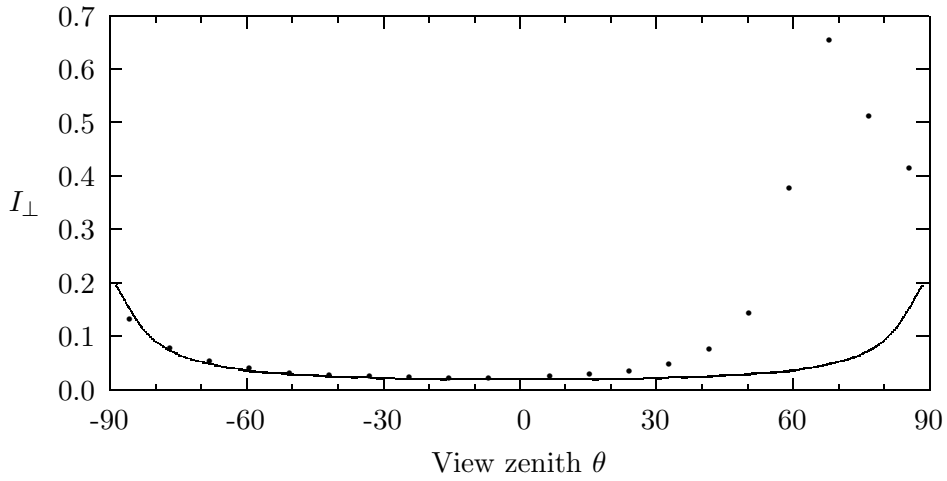

Figure 37: Horizontally polarized component of the radiance in the principal plane. The line represents the result for a Rayleigh atmosphere with $\tau_m = 0.1$ over a Lambert surface with albedo $A = 0.25$, while the dots show the effect of adding aerosol with optical thickness $\tau_a = 0.1$ and scattering properties as described in the text. Note the symmetry of the Rayleigh component.